Supporting Information (SI)

Ferrocene-Based Heteroditopic Receptors Displaying High Selectivity toward Lead and Mercury Metal Cations through Different Channel

María Alfonso, Alberto Tárraga, * and Pedro Molina*

Departamento de Química Orgánica. Facultad de Química. Universidad de Murcia.

Campus de Espinardo, E-30100 Murcia, Spain.

E-mail: pmolina@um.es; atarraga@um.es

Table of contents

NMR spectra of **2**, **3**, **4** and **7** S4

Figure S1. Evolution of CV and OSWV of **4** in the presence of increasing amounts of $Pb(ClO_4)_2$ in CH_3CN. S14

Figure S2. Evolution of the LSW of **4** in the presence of increasing amountsof several cations in CH_3CN S15

Figure S3. Evolution of the LSW of **7** in the presence of increasing amountsof $Hg(OTf)_2$ and $Cu(OTf)_2$ in CH_3CN S16

Figure S4. Evolution of OSWV of **4** in the presence of increasing amounts of $[(n\text{-}Bu)_4]H_2PO_4$ and 20 equivalent of acetic acid in CH_3CN S16
Figure S5. Evolution of OSWV of **4** in the presence of increasing amounts of $[(n\text{-}Bu)_4]_3HP_2O_7$ and $[(n\text{-}Bu)_4N]F$ in absence and in the presence of 20 equivalent of acetic acid in CH_3CN S17
Figure S6. Evolution of the OSWV of **4** in the presence of increasing amounts of $[(n\text{-}Bu)_4\ N]OH$ in CH_3CN S18
Figure S7. Evolution of OSWV of **7** in the presence of increasing amounts of $[(n\text{-}Bu)_4\ N]H_2PO_4$ and 20 equivalent of acetic acid in CH_3CN S18
Figure S8. Evolution of OSWV of **7** in the presence of increasing amounts of $[(n\text{-}Bu)_4\ N]_3HP_2O_7$ and $[(n\text{-}Bu)_4\ N]AcO$ in absence and in the presence of 20 equivalent of acetic acid in CH_3CN S19
Figure S9. Evolution of OSWV of **7** in the presence of increasing amounts of $[(n\text{-}Bu)_4N]F$ in absence and in the presence of 20 equivalent of acetic acid in CH_3CN S20
Figure S10. Evolution of the OSWV of **7** in the presence of increasing amounts of $[(n\text{-}Bu)_4\ N]OH$ in CH_3CN S20
Table S1. Electrochemical data of receptor **4** and **7** in the presence of anions S21
Figure S11. Evolution of the OSWV of **4** in the presence of several anions and Pb^{2+} in CH_3CN S21
Figure S12. Evolution of the OSWV of **7** in the presence of several anions and Hg^{2+} in CH_3CN S22
Figure S13. Changes in the absorption spectrum of **4** upon addition of increasing amounts of $Hg(OTf)_2$ and $Cu(OTf)_2$ and in CH_3CN S22
Figure S14. Changes in the absorption spectrum of **7** upon addition of increasing amounts of $Cu(OTf)_2$ in CH_3CN S23
Figure S15. Changes in the absorption spectrum of **4** upon addition of increasing amounts of $[(n\text{-}Bu)_4\ N]AcO$ and $[(n\text{-}Bu)_4\ N]H_2PO_4$ in CH_3CN S23
Figure S16. Changes in the absorption spectrum of **4** upon addition of increasing amounts of several anions in absence and in the presence of 20 equivalent of acetic acid in CH_3CN S24
Figure S17. Changes in the absorption spectrum of **4** upon addition of increasing amounts of $[(n\text{-}Bu)_4\ N]AcO$ and $[(n\text{-}Bu)_4\ N]H_2PO_4$ in CH_3CN S25
Figure S18. Changes in the absorption spectrum of **7** upon addition of increasing amounts of $[(n\text{-}Bu)_4\ N]_3HP_2O_7$ in absence and in the presence of 20 equivalent of acetic acid in CH_3CN S25
Figure S19. Changes in the absorption spectrum of **7** upon addition of increasing amounts of $[(n\text{-}Bu)_4\ N]F$ in absence and in the presence of 20 equivalent of acetic acid and $[(n\text{-}Bu)_4\ N]OH$ in CH_3CN S26
Figure S20. Change of absorbance of **4** upon addition of $Pb(ClO_4)_2$ and $Hg(OTf)_2$ indicating the stoichiometry formation of complexes S27
Figure S21. Reversibility experiment for compound **4**. S27
Figure S22. Semilogarithmic plot for determining the detection limit of **4** towards $Pb(ClO_4)_2$ and $Hg(OTf)_2$ S28
Figure S23. Semilogarithmic plot for determining the detection limit of **7** towards $Hg(OTf)_2$ S28
Table S2. UV-vis data for receptors **4** and **7** in the presence of several cations and anions S29
Figure S24. Fluorescence intensity of ligands **4** in CH_3CN after addition of several cations and fluorescence emission intensity of **4** upon addition of 1 equiv of $Pb(ClO_4)_2$ in the presence of 1 equiv of interference metal ions in CH_3CN S30
Figure S25. Changes in the fluorescence emission of **4** upon addition of $Pb(ClO_4)_2$ in CH_3CN and visual features observed in the CH_3CN solutions addition of $Pb(ClO_4)_2$ S30

Figure S26 Semilogarithmic plot for determining the detection limit of **4** towards $Pb(ClO_4)_2$ S31
Table S3. Fluorescence data for receptor **4** in the presence of $Pb(ClO4)_2$ in CH_3CN solution S31
Figure S27. Fluorescence intensity of ligands **7** in CH_3CN after addition of several cations and fluorescence emission intensity of **7** upon addition of 2 equiv of $Hg(OTf)_2$ in the presence of 2 equiv of interference metal ions in CH_3CN S31
Figure S28. Semilogarithmic plot for determining the detection limit of **7** towards $Hg(OTf)_2$ S32
Chart 1. Schematic representation of the binding mode between Hg^{2+} and **4**. S32
Table S4. ^{1}H-NMR titration data for receptor **4** in the presence of $Pb(ClO_4)_2$, $([n\text{-}Bu)_4\ N]AcO$ and $[(n\text{-}Bu)_4]H_2PO_4$ in CH_3CN solution S33
Figure S29. Changes in the ^{1}H-NMR spectrum of **4** upon addition of increasing amounts of $([n\text{-}Bu)_4\ N]AcO$ S33
Figure S30. Changes in the ^{1}H-NMR spectrum of **4** upon addition of increasing amounts of $([n\text{-}Bu)_4\ N]\ H_2PO_4$ S34
Table S5. ^{1}H-NMR titration data for receptor **7** in the presence of $Hg(OTf)_2$, $([n\text{-}Bu)_4]AcO$ and $[(n\text{-}Bu)_4\ N]H_2PO_4$ in CH_3CN in DMSO solution S34
Figure S31. Changes in the ^{1}H-NMR spectrum of **7** upon addition of increasing amounts of $([n\text{-}Bu)_4\ N]AcO$ S35
Figure S32. Changes in the ^{1}H-NMR spectrum of **7** upon addition of increasing amounts of $([n\text{-}Bu)_4\ N]\ H_2PO_4$ S35
Figure S33. Relative abundance of the isotopic cluster of the complex for **4**·with $Pb(ClO4)_2$ and $Hg(OTf)_2$ S36
Figure S34. Relative abundance of the isotopic cluster of the complex for **7**·with $Hg(OTf)_2$ S37
Figure S35. ESI-MS spectra of an acetonitrilo solution of an equimolecular amount of $[(n\text{-}Bu)_4]AcO$ and ligand **4** S38
Figure S36. ESI-MS spectra of an acetonitrilo solution of an equimolecular amount of $[(n\text{-}Bu)_4]AcO$ and ligand **4** S38
Figure S37. ESI-MS spectra of an acetonitrilo solution of an equimolecular amount of $[(n\text{-}Bu)_4]AcO$ and $Pb(ClO_4)_2$ and ligand **4** S39
Figure S38. ESI-MS spectra of an acetonitrilo solution of an equimolecular amount of $[(n\text{-}Bu)_4]AcO$ and ligand **7** S39
Figure S39. ESI-MS spectra of an acetonitrilo solution of an equimolecular amount of $[(n\text{-}Bu)_4]AcO$ and ligand **7** S40
Figure S40. Changes in the fluorescence emission spectrum of **4** and of the complex $[\mathbf{4}\cdot Pb^{2+}]$ upon addition of several anions. S42
Figure S41. Changes in the fluorescence emission spectrum of **7** and of the complex $[\mathbf{7}\cdot Hg^{2+}]$ upon addition of several anions. S41
General Comments S42

6-amino-7-nitrodibenzo[a,c]phenazine 2

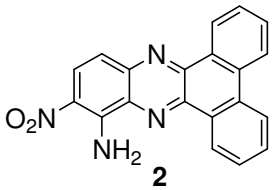

2

^{1}H NMR (400 MHz, DMSO-d^6)

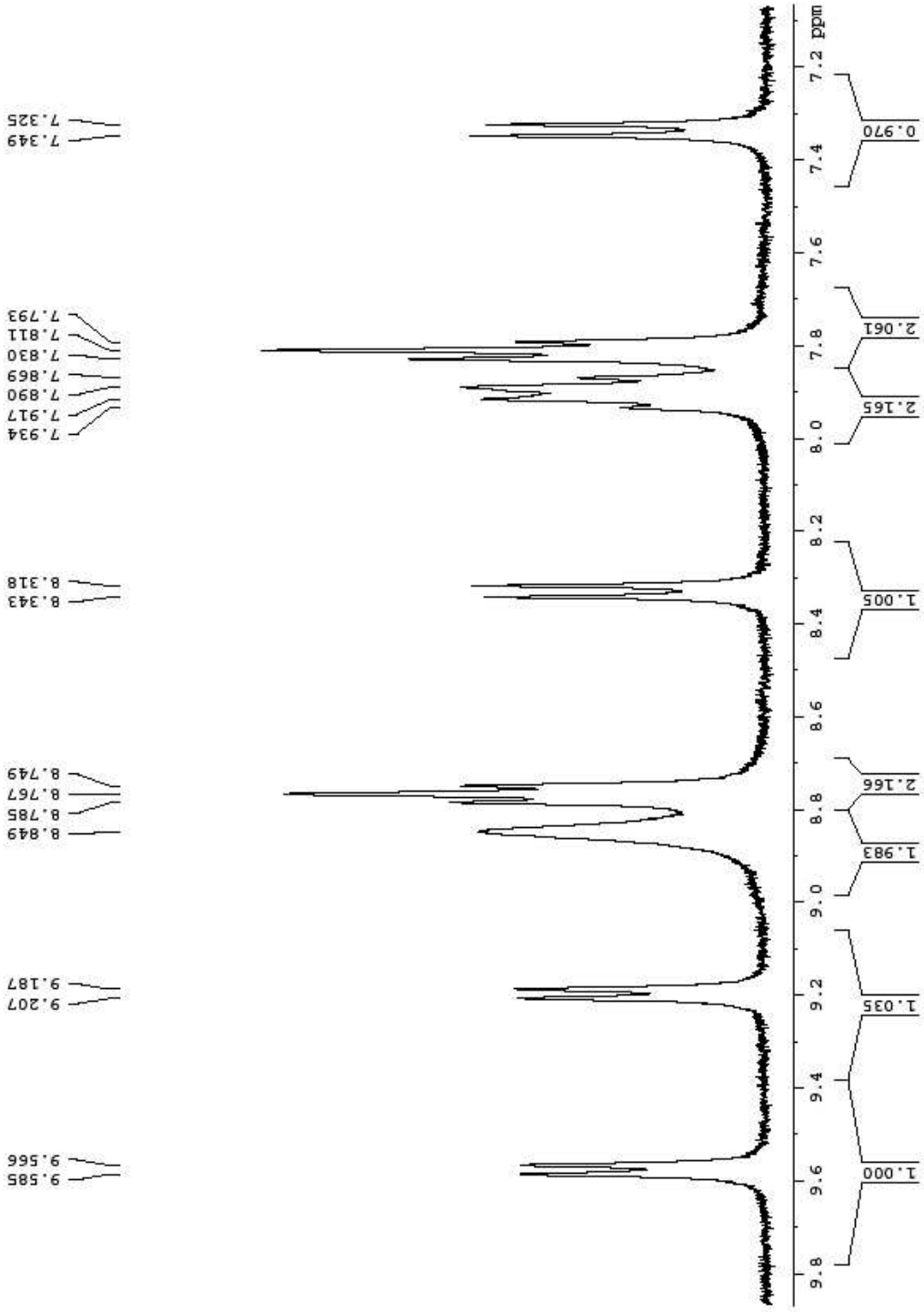

^{13}C NMR (100 MHz, DMSO-d^{6})

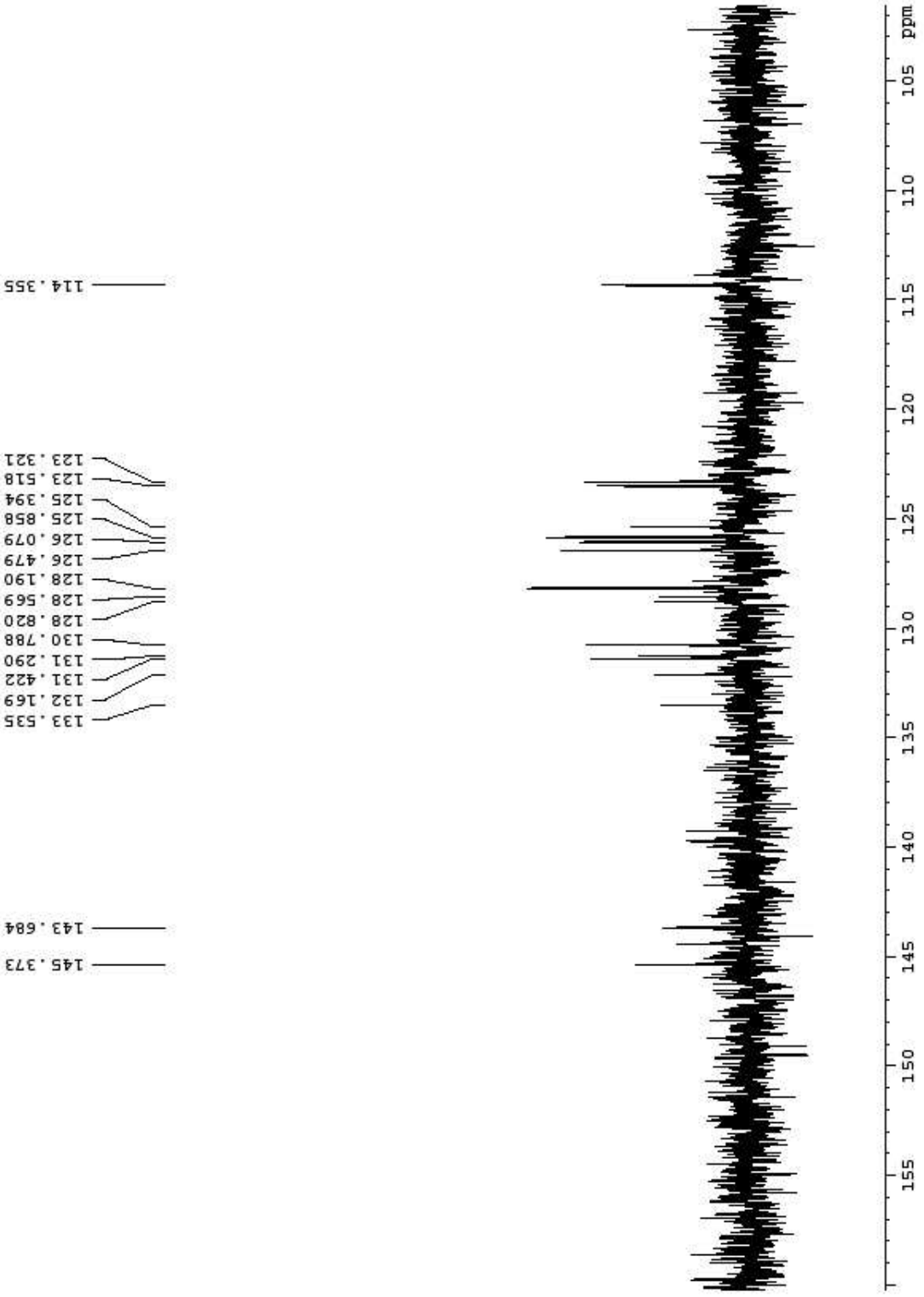

6-7-diaminodibenzo[a,c]phenazine 3

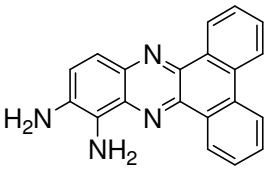

^{1}H NMR (400 MHz, DMSO-d^{6})

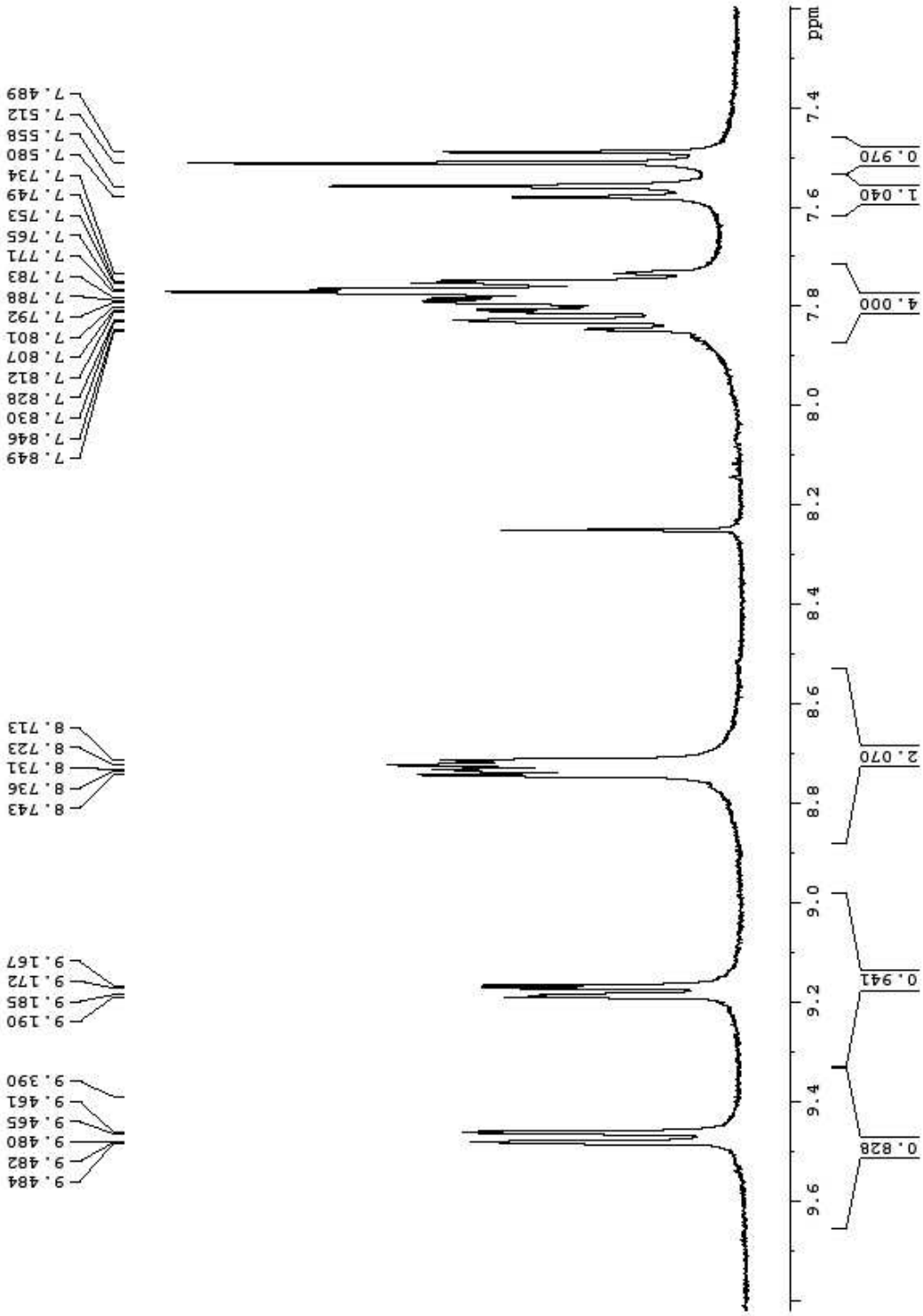

^{13}C NMR (100 MHz, DMSO-d^{6})

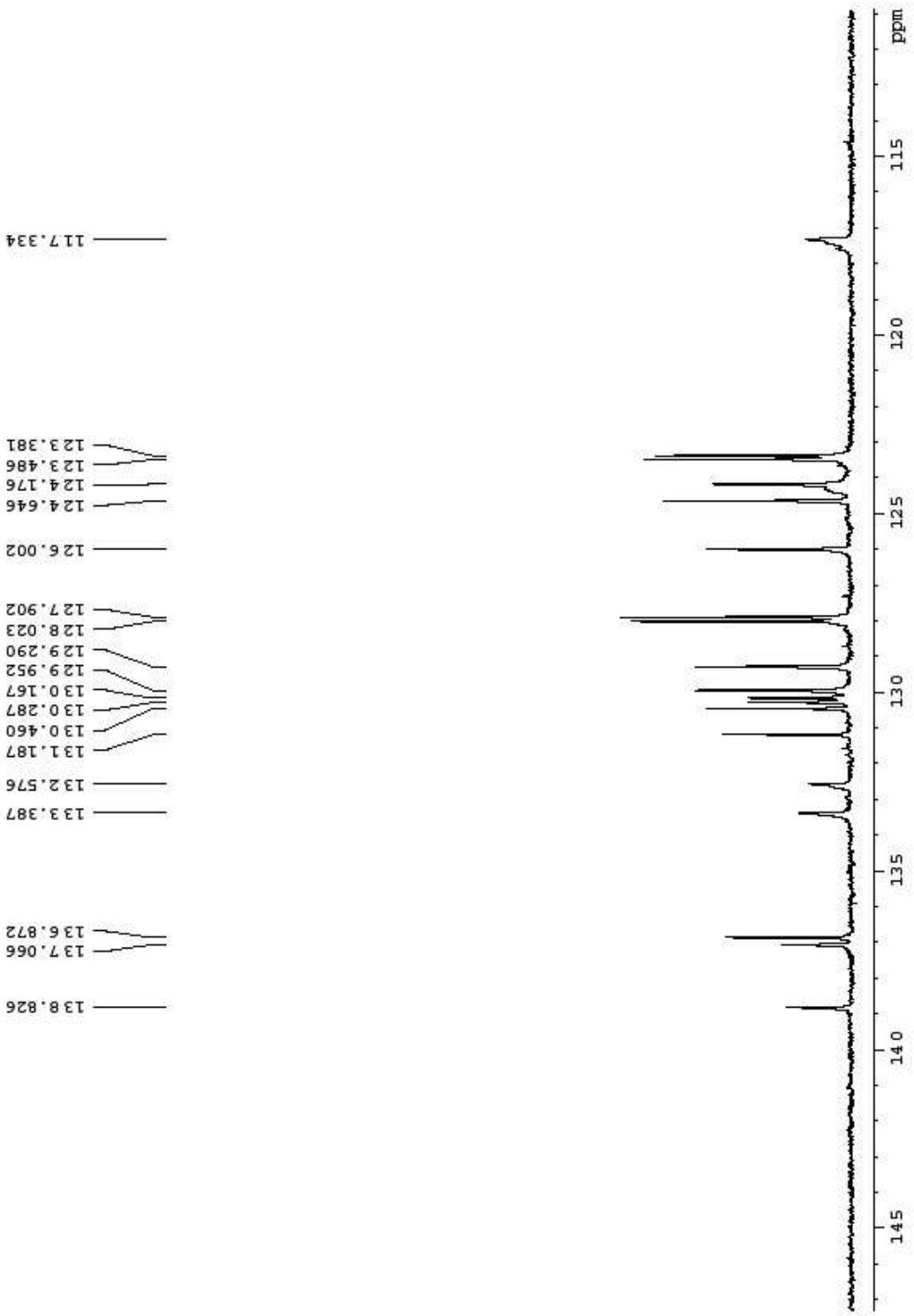

2-Ferrocenyl-3*H*-dibenzo[a, c]imidazo[4,5-*h*]phenazine 4

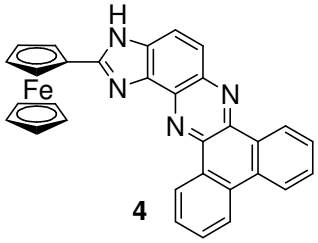

4

^{1}H NMR (400 MHz, DMSO-d^6)

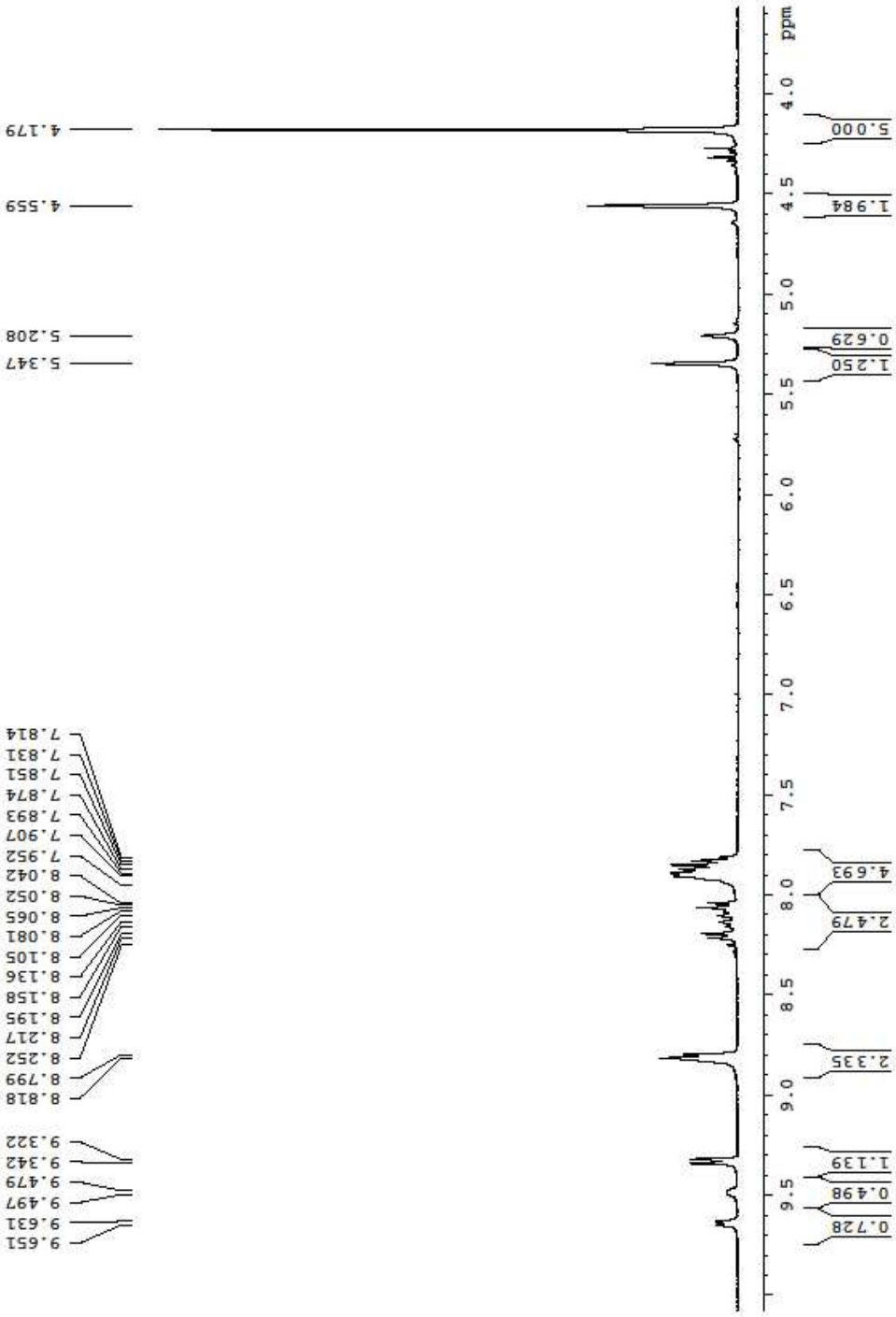

^{13}C NMR (100 MHz, DMSO-d^{6})

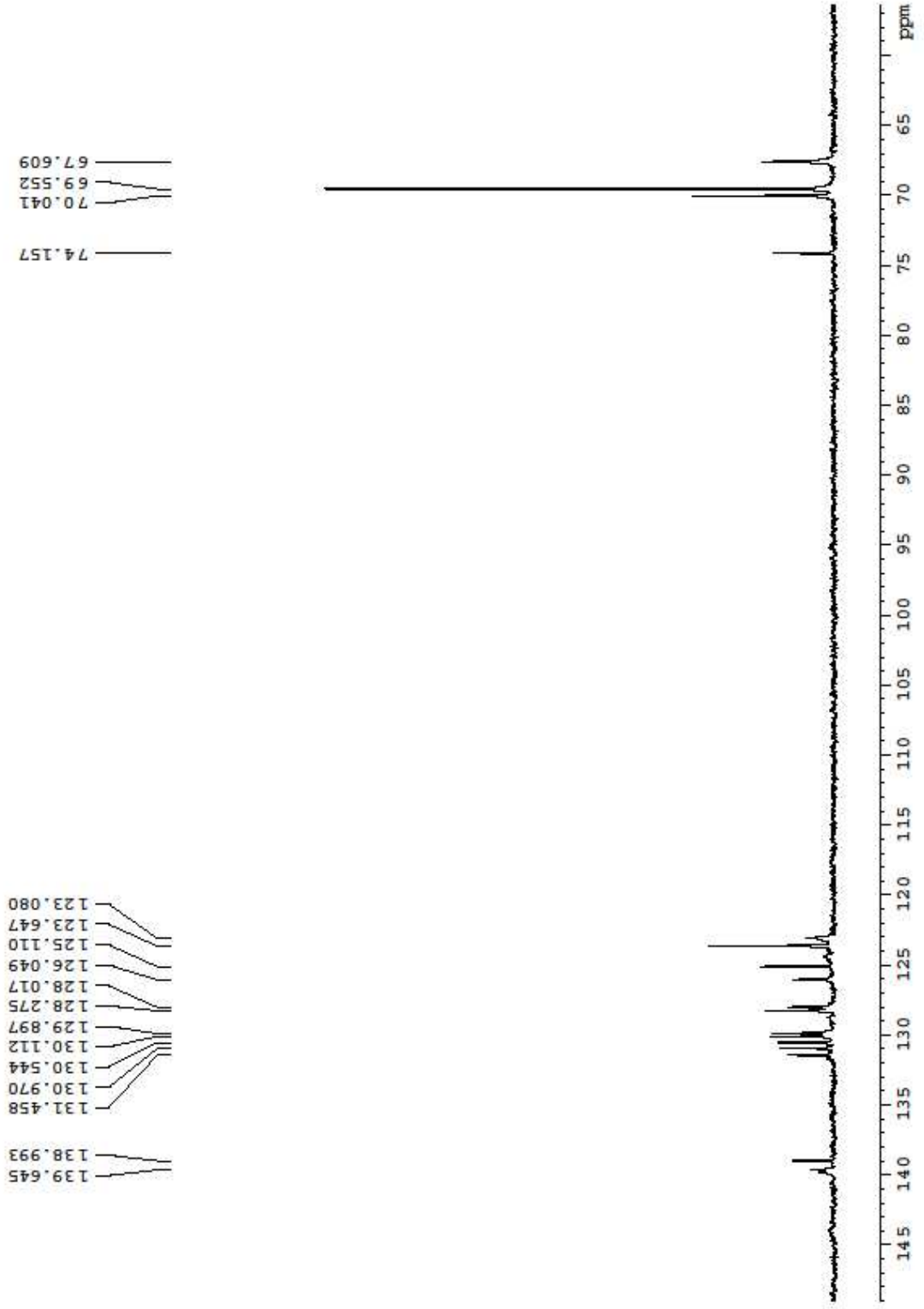

2-Ferrocenyl-4,5-diamino-1H-benzo[d]imidazol 6

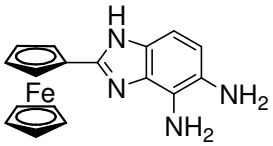

^{1}H NMR (300 MHz, DMSO-d^6)

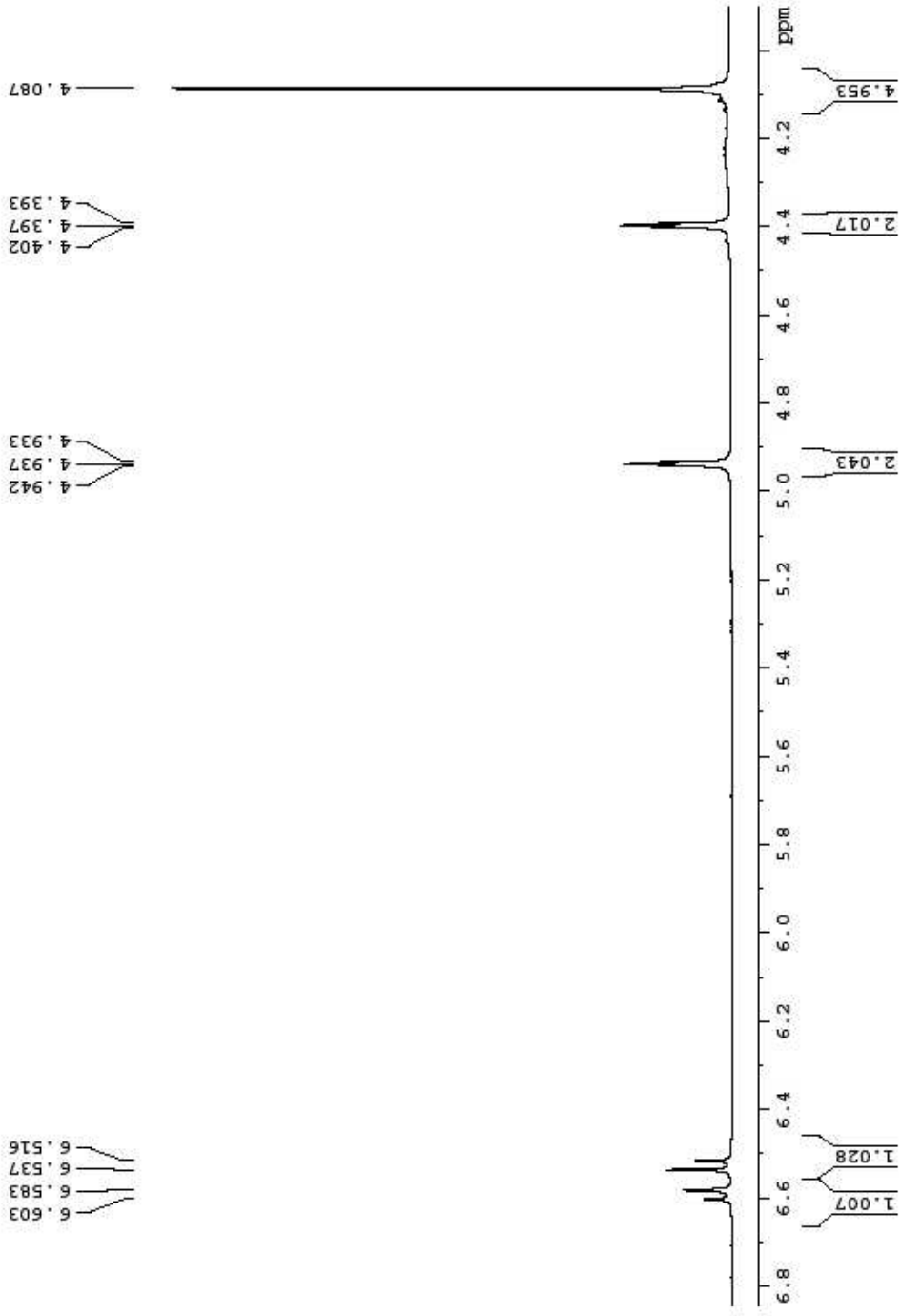

^{13}C NMR (75MHz, DMSO-d^{6})

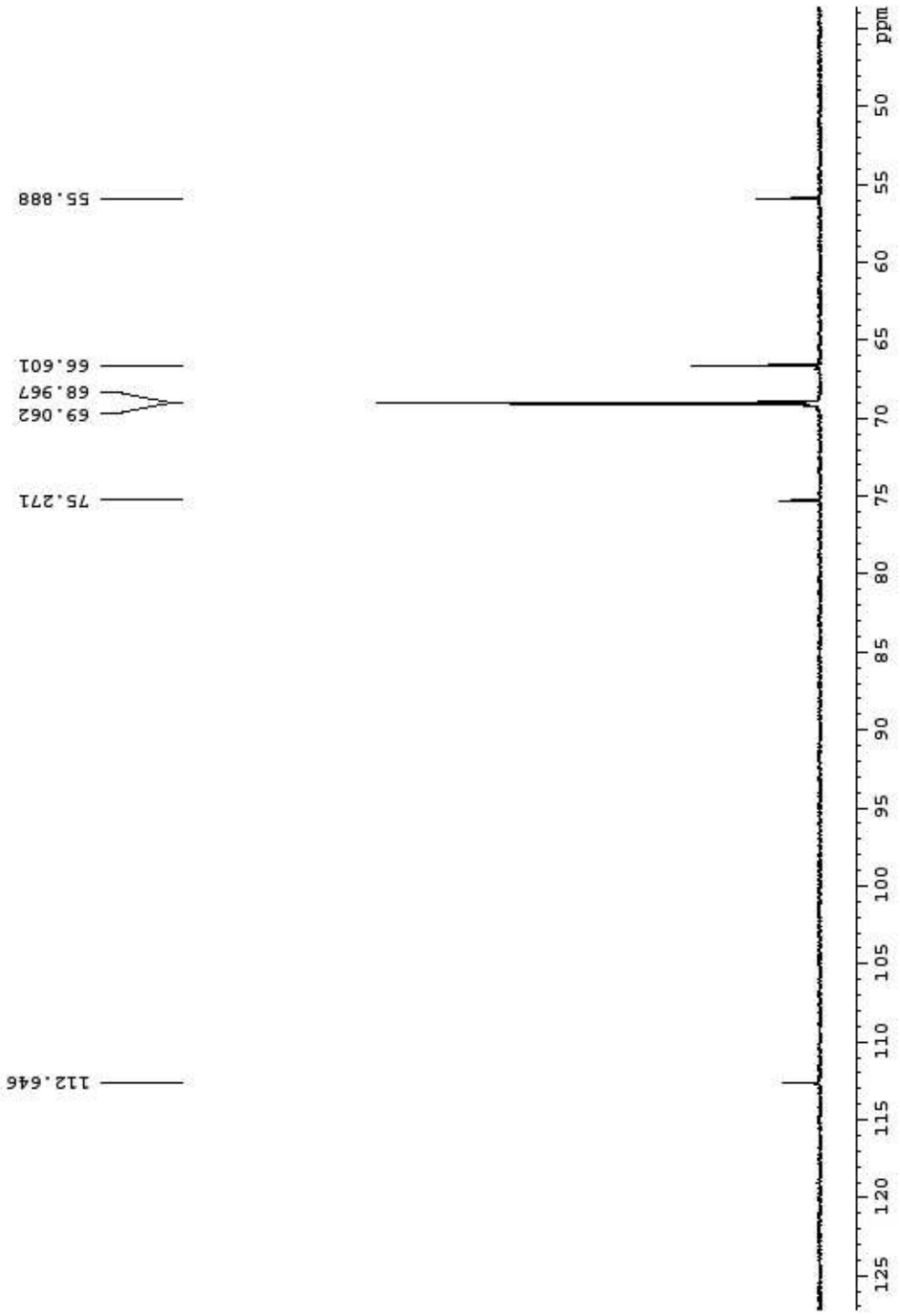

2-Ferrocenyl-3*H*-dipyrido[3,2-a:2',3'-c]imidazo[4,5-*h*]phenazine 7

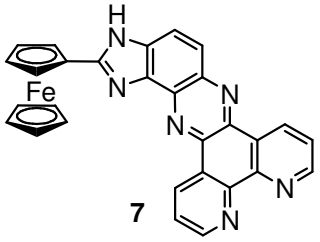

7

^{1}H NMR (400 MHz, DMSO-d^6)

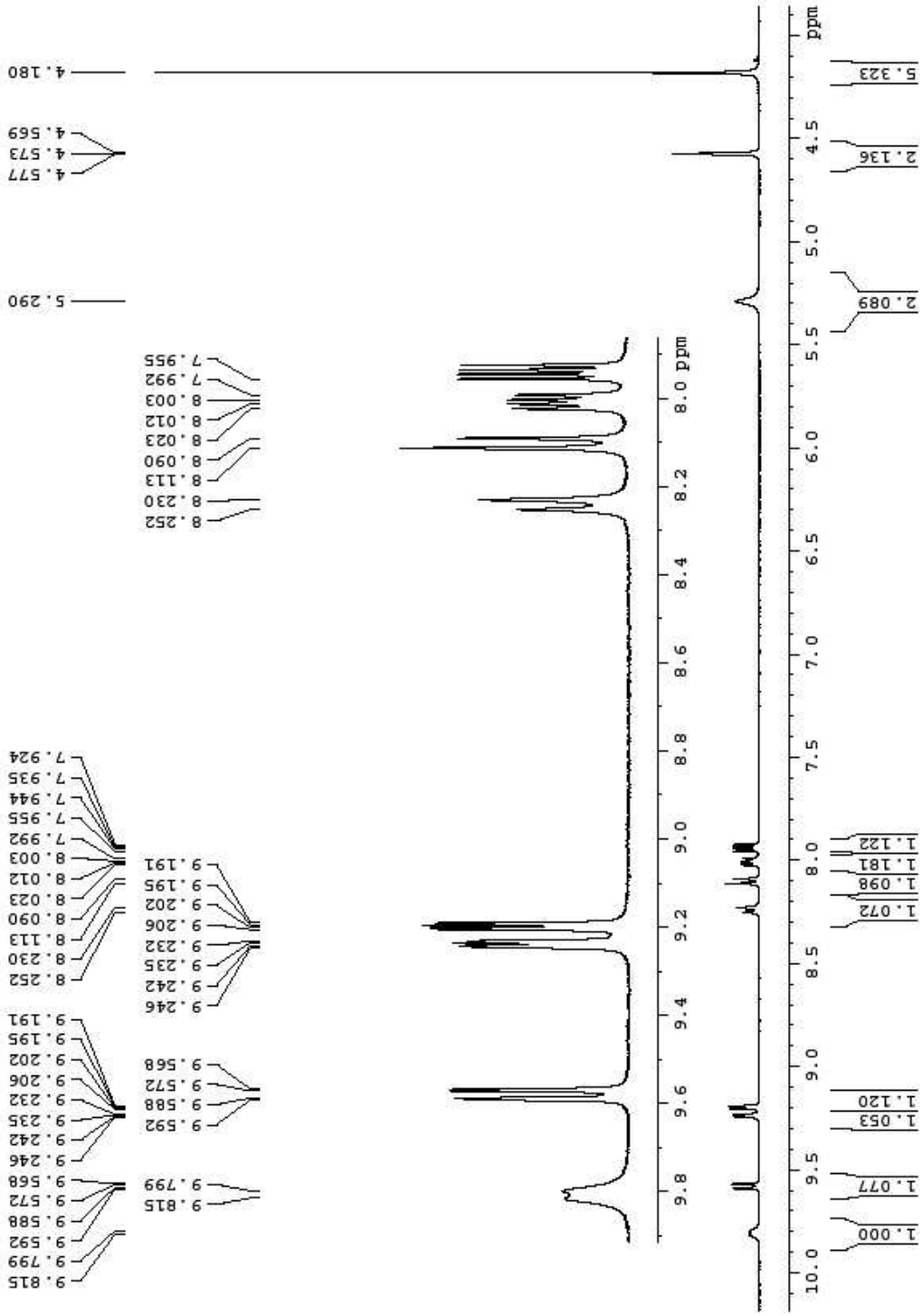

^{13}C NMR (100 MHz, DMSO-d^{6})

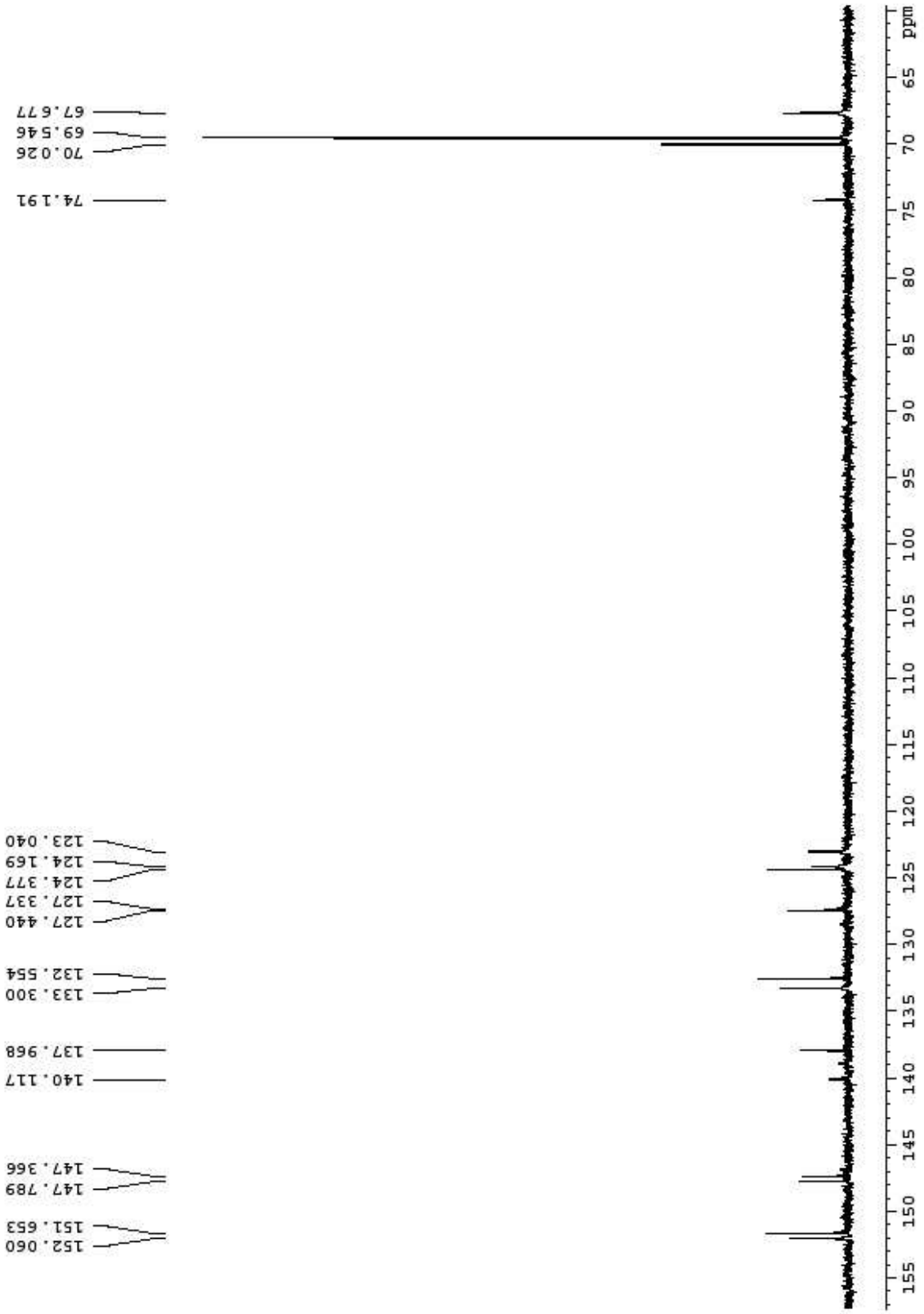

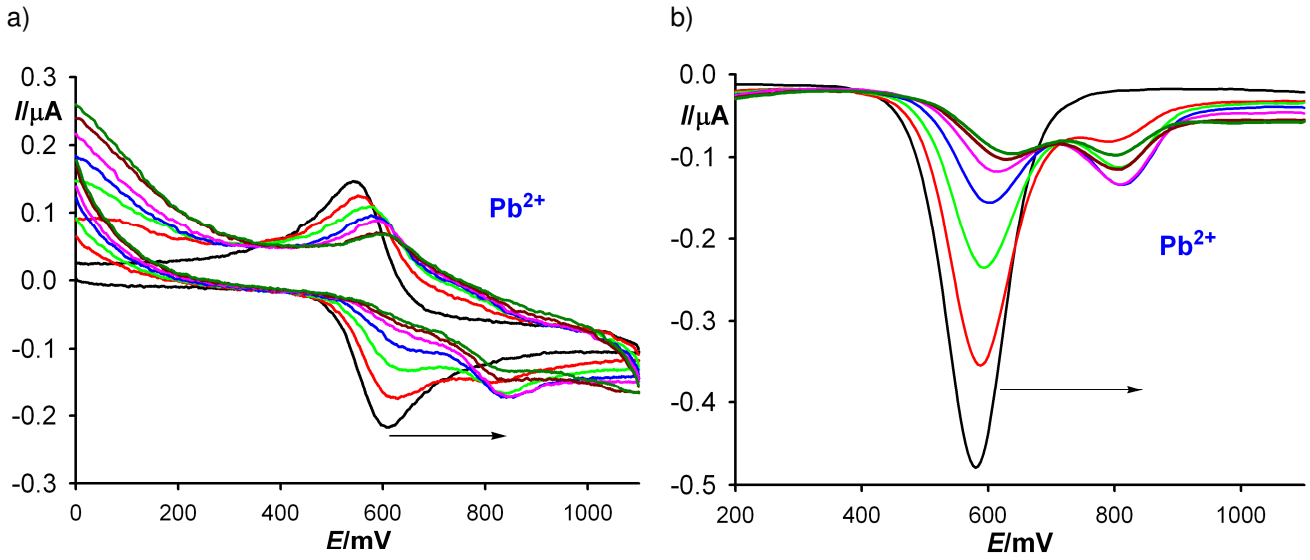

Figure S1. Evolution of the CV (a) and OSWV (b) of **4** ($5x10^{-4}$ M) in $CH_3CN/[(n\text{-}Bu)_4]PF_6$ scanned at 0.1 V s^{-1} in the presence of increasing amounts of $Pb(ClO_4)_2$.

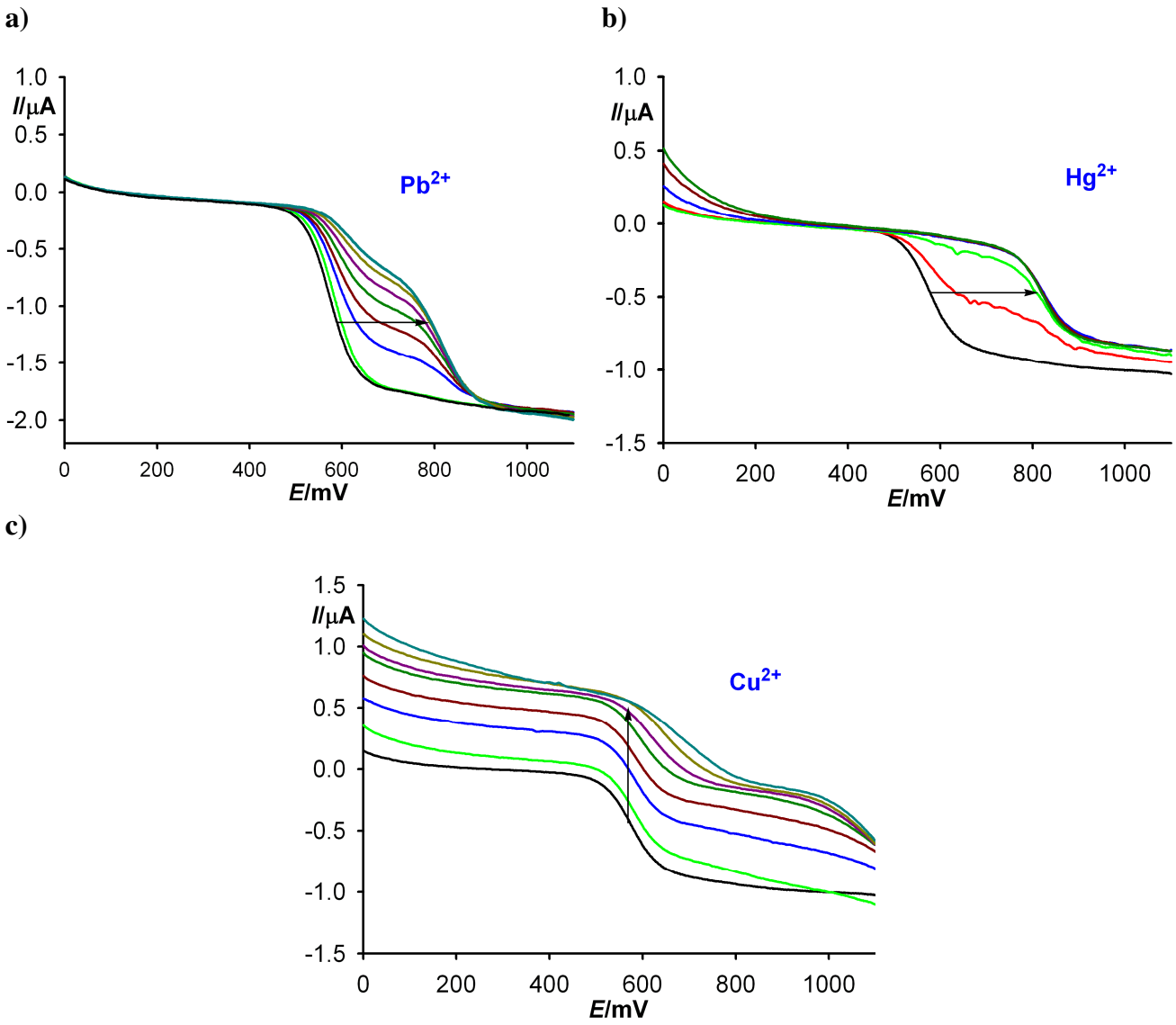

Figure S2. Evolution of the LSW of **4** ($5x10^{-4}$ M in CH_3CN) in the presence of increasing amounts of (a) $Pb(ClO_4)_2$; (b) $Hg(OTf)_2$; (c) $Cu(OTf)_2$, obtained using a rotating disk electrode at 100 mVs^{-1} and 1000 rpm and $[(n\text{-}Bu)_4 N]PF_6$ 0.1 M as supporting electrolyte.

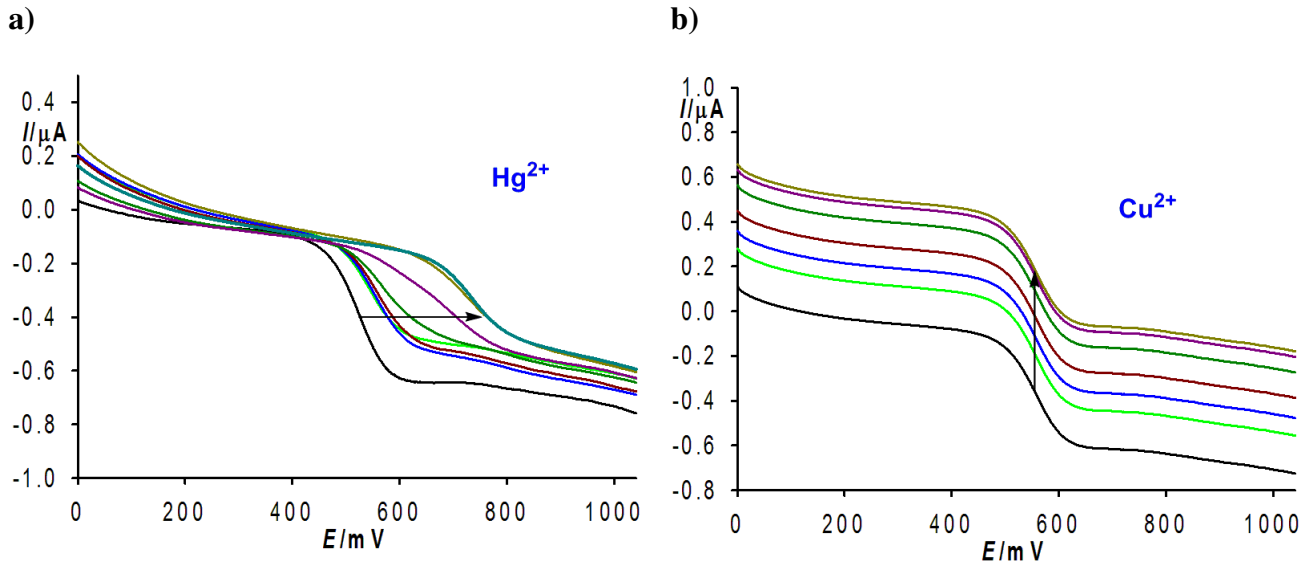

Figure S3. Evolution of the LSW of **7** ($1x10^{-4}$ M in CH_3CN) in the presence of increasing amounts of (a) $Hg(OTf)_2$; (b) $Cu(OTf)_2$, obtained using a rotating disk electrode at 100 mVs^{-1} and 1000 rpm and $[(n\text{-}Bu)_4\ N]PF_6$ 0.1 M as supporting electrolyte.

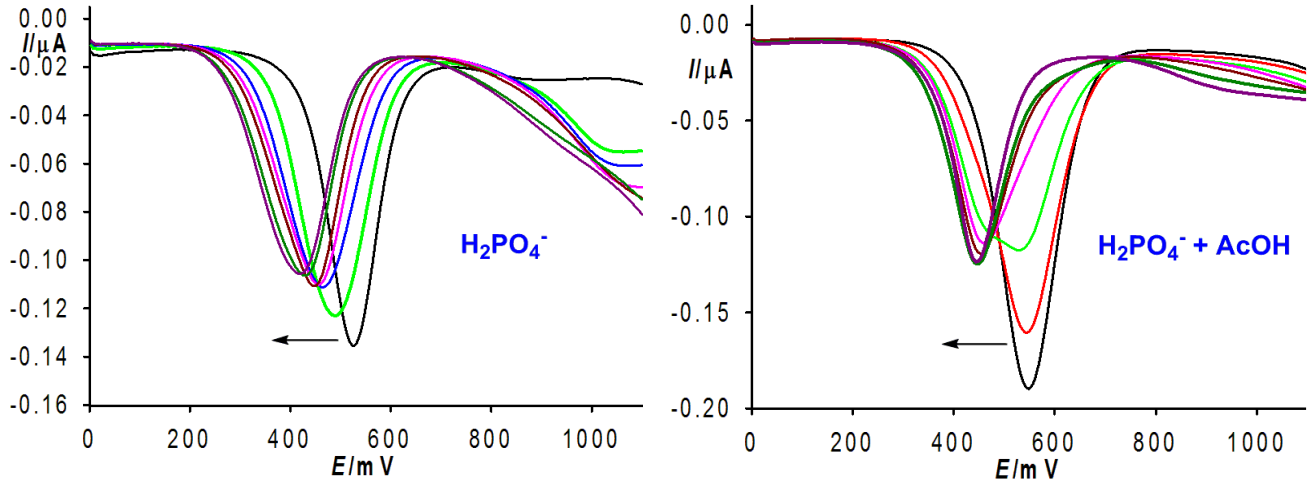

Figure S4. Evolution of the OSWV of **4** ($5x10^{-4}$ M) in $CH_3CN/[(n\text{-}Bu)_4\ N]PF_6$ scanned at 0.1 V s^{-1} in the presence of increasing amounts of (a) $H_2PO_4^-$ until 3 equiv (left) and in the presence of 3 equiv. of $H_2PO_4^-$ and 20 equiv of acetic acid (right).

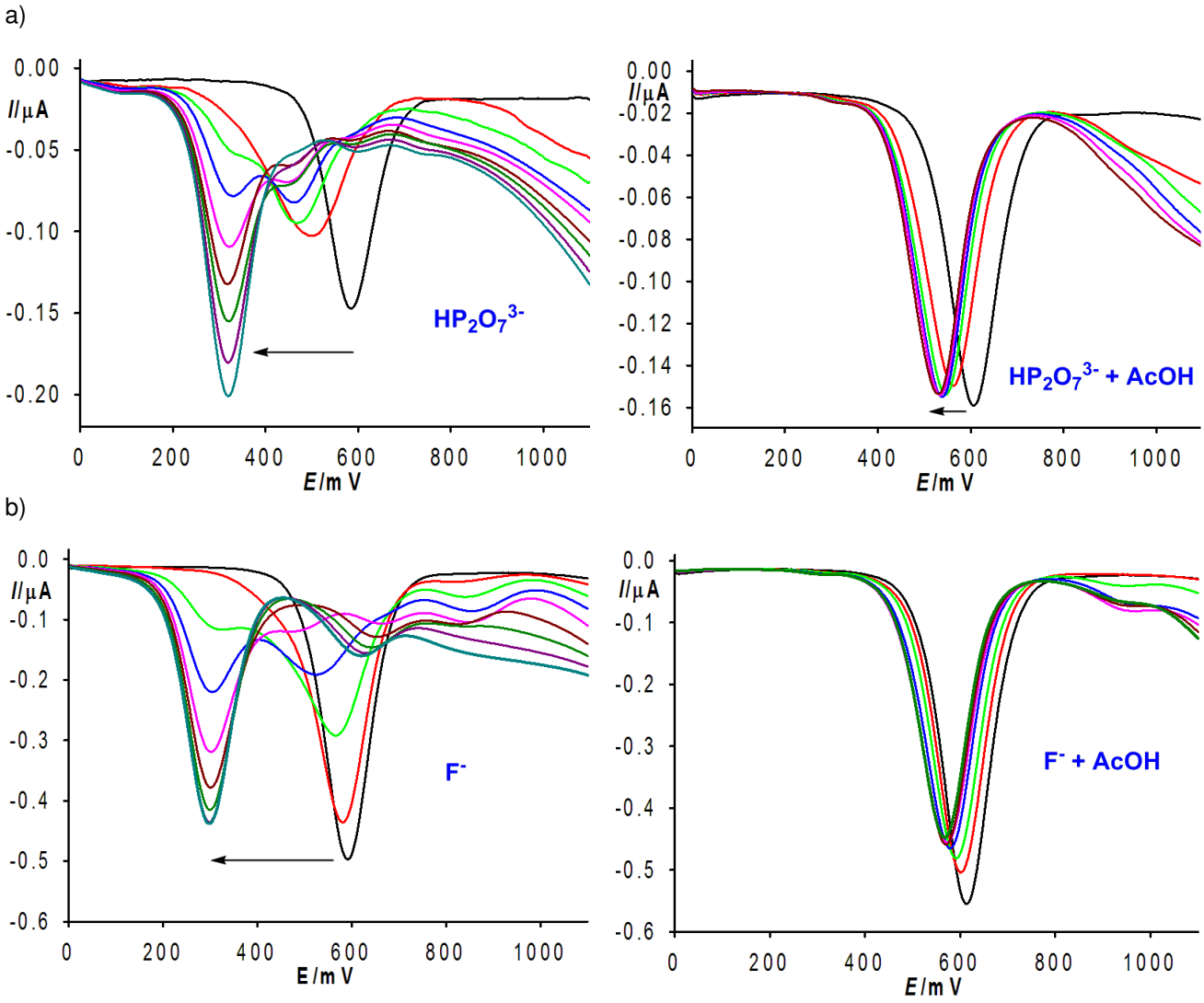

Figure S5. Evolution of the OSWV of **4** ($5\cdot10^{-4}$ M) in $CH_3CN/[(n\text{-}Bu)_4N]PF_6$ scanned at 0.1 V s^{-1} in the presence of increasing amounts of:(a) $HP_2O_7^{3-}$ (left) until 3 equiv. and in the presence of 3 equiv. of $HP_2O_7^{3-}$ and 20 equiv of acetic acid (right); (b) F^- until 3 equiv (left) and in the presence of 3 equiv. of F^- and 20 equiv of acetic acid (right).

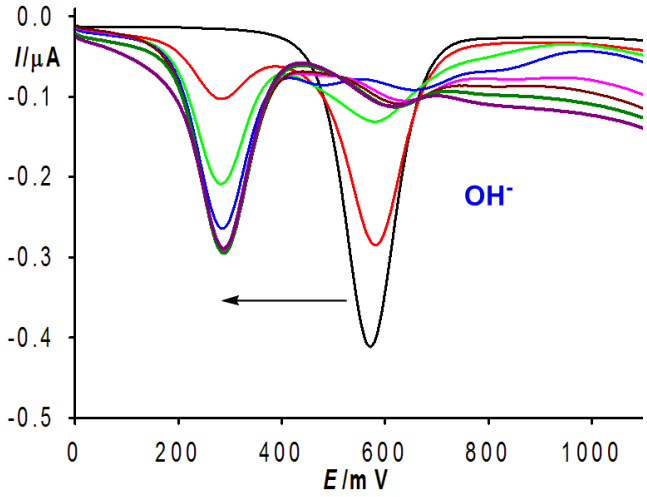

Figure S6. Evolution of the OSWV of **4** ($5x10^{-4}$ M) in $CH_3CN/[(n\text{-}Bu)_4\ N]PF_6$ scanned at 0.1 V s^{-1} in the presence of increasing amounts of OH^- until 2 equiv.

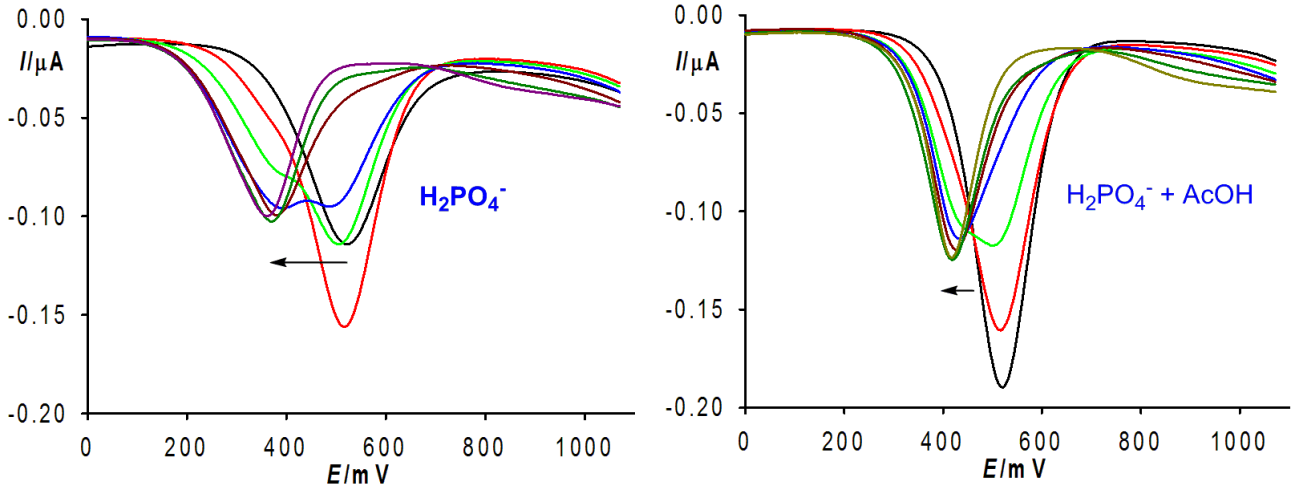

Figure S7. Evolution of the OSWV of **7** ($1x10^{-4}$ M) in $CH_3CN/[(n\text{-}Bu)_4\ N]PF_6$ scanned at 0.1 V s^{-1} in the presence of increasing amounts of $H_2PO_4^-$ until 3 equiv. (left) and in the presence of 20 equiv. of acetic acid (right).

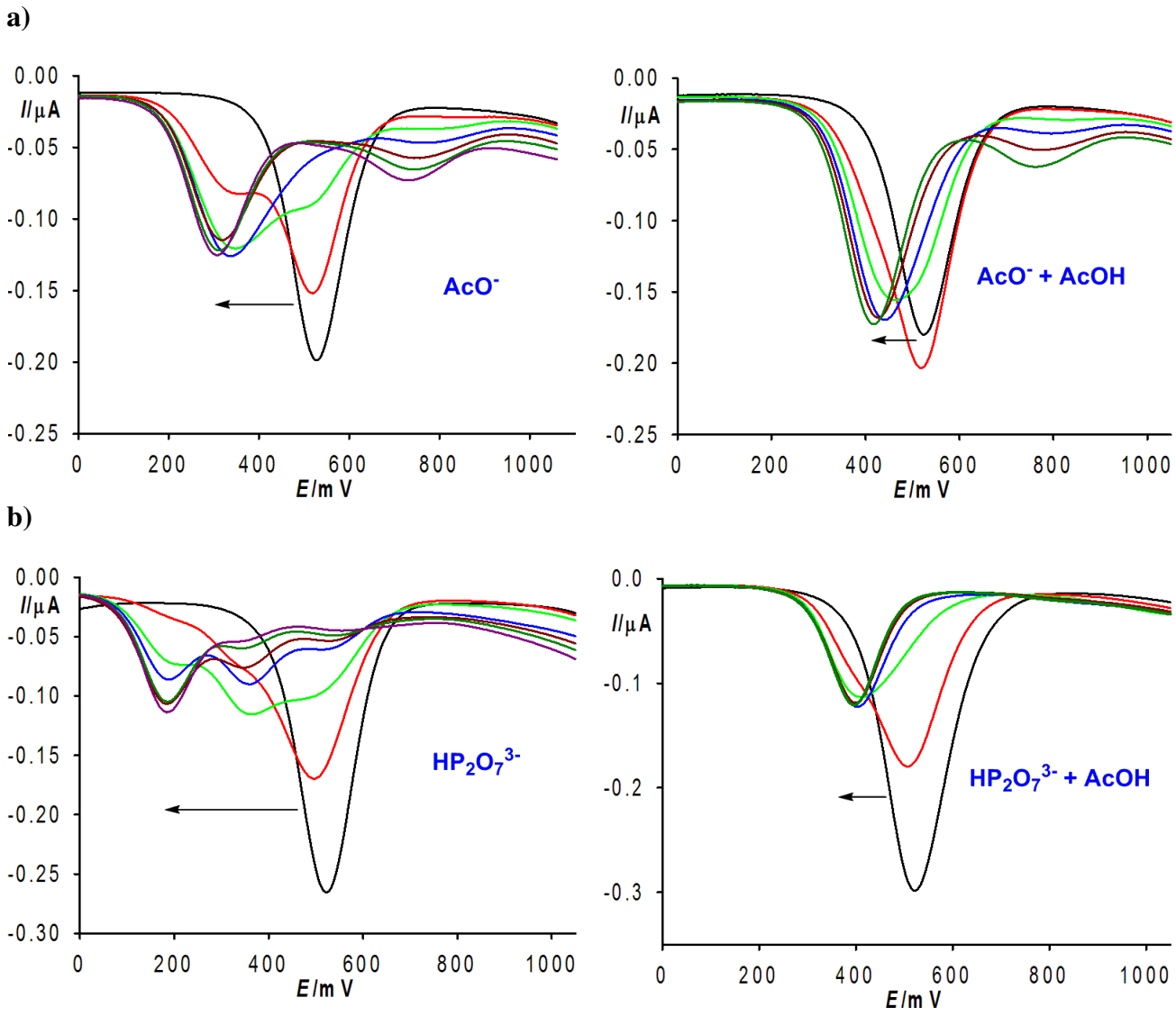

Figure S8. (a) Evolution of the OSWV of **7** ($1x10^{-4}$ M) in $CH_3CN/[(n\text{-}Bu)_4N]PF_6$ scanned at 0.1 V s^{-1} in the presence of increasing amounts of (a) AcO^- until 3 equiv (left) and in the presence of 3 equiv. of AcO^- and 20 equiv of acetic acid (right); (b) $HP_2O_7^{3-}$ until 3 equiv (left) and in the presence of 3 equiv. of $HP_2O_7^{3-}$ and 20 equiv of acetic acid (right).

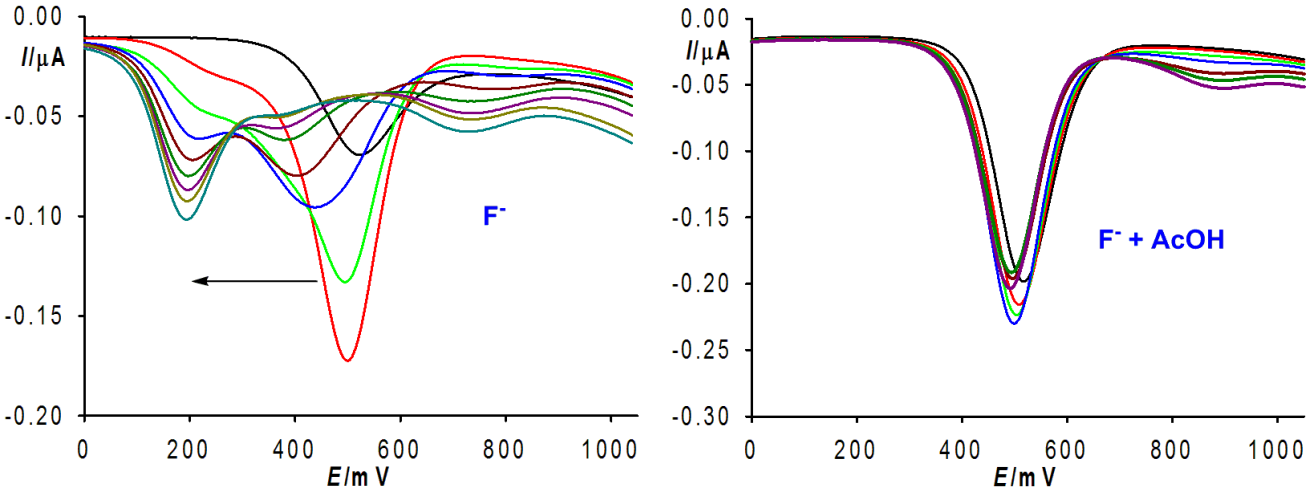

Figure S9. Evolution of the OSWV of **7** ($1x10^{-4}$ M) in $CH_3CN/[(n\text{-}Bu)_4\ N]PF_6$ scanned at 0.1 V s^{-1} in the presence of increasing amounts of F^- (left) until 3 equiv. and in the presence of 3 equiv. of F^- and 20 equiv of acetic acid (right).

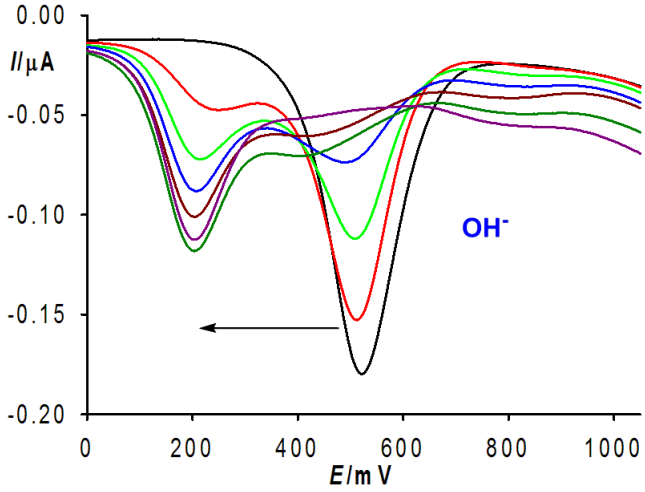

Figure S10. Evolution of the OSWV of **7** ($1x10^{-4}$ M) in $CH_3CN/[(\ n\text{-}Bu)_4\ N]PF_6$ scanned at 0.1 V s^{-1} in the presence of increasing amounts of OH^- until 2 equiv.

Table SI 1. Electrochemical data of receptor **4** and **7** in the presence of anions.

Receptor	Anion added	$E_{1/2}$ (V)	Acid added[d]	$\Delta E_{1/2}$ (mV)
4		0.58		
4	AcO-	0.46[a]	no	-120
4	AcO-	0.51 [a]	yes	-70
4	$H_2PO_4^-$	0.47 [a]	no	-110
4	$H_2PO_4^-$	0.51 [a]	yes	-70
4	$HP_2O_7^{3-}$	0.46 [b]	no	-120
4	$HP_2O_7^{3-}$	0.29 [a]	no	-290
4	$HP_2O_7^{3-}$	0.50[a]	yes	-80
4	F^-	0.29 [a]	no	-290
4	F^-	0.58 [a]	yes	0
4	OH^-	0.29[c]		-290
7		0.52		
7	AcO-	0.30 [a]	no	-220
7	AcO-	0.41 [a]	yes	-110
7	$H_2PO_4^-$	0.36 [a]	no	-160
7	$H_2PO_4^-$	0.42 [a]	yes	-100
7	$HP_2O_7^{3-}$	0.35 [b]	no	-170
7	$HP_2O_7^{3-}$	0.19 [a]	no	-330
7	$HP_2O_7^{3-}$	0.39 [a]	yes	-130
7	F^-	0.19 [a]	no	-330
7	F^-	0.52 [a]	yes	0
7	OH^-	0.19[c]		-330

[a]: 3 equiv added; [b]: 1 equiv added; [c]: 2 equiv added; [d]: 20 equiv of acetic acid added

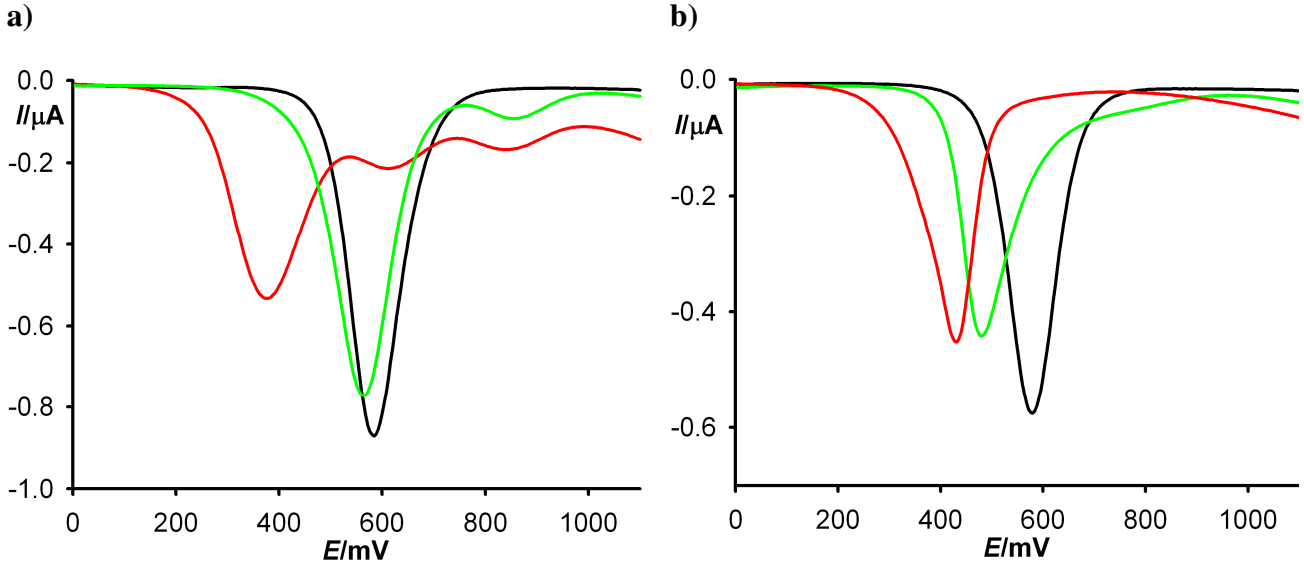

Figure S11. (a) Evolution of the OSWV of **4** (black) ($5x10^{-4}$ M in CH_3CN) [$(n\text{-}Bu)_4N]PF_6$ scanned at 0.1 V s^{-1} in the presence of 3 equiv of AcO^- (red) and in the presence of 3 equiv of AcO^- and 1 equiv of Pb^{2+} (green). (b) Evolution of the OSWV of **4** (black) ($5x10^{-4}$ M in CH_3CN) [$(n\text{-}Bu)_4N]PF_6$] scanned at 0.1 V s^{-1} in the presence of 3 equiv of $H_2PO_4^-$ (red) and in the presence of 3 equiv of $H_2PO_4^-$ and 1 equiv of Pb^{2+} (green).

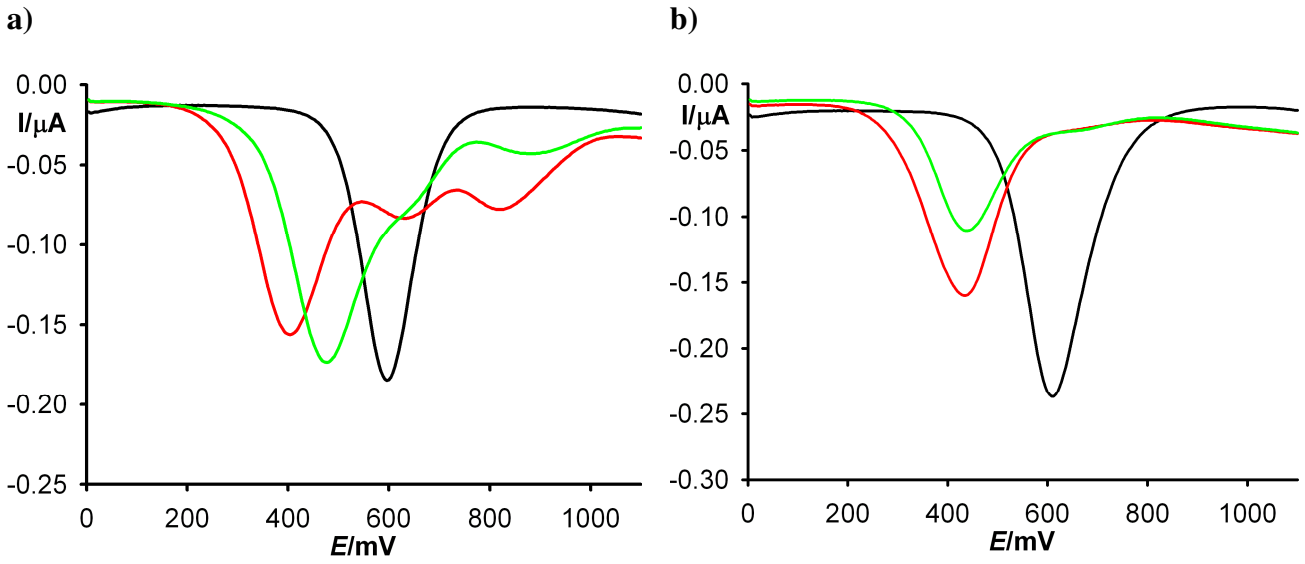

Figure S12. (a) Evolution of the OSWV of **7** (black) ($5x10^{-4}$ M in CH_3CN) [(n-Bu)$_4$ N]PF_6] scanned at 0.1 V s^{-1} in the presence of 3 equiv of AcO^- (red) and in the presence of 3 equiv of AcO^- and 0.5 equiv of Hg^{2+} (green). (b) Evolution of the OSWV of **7** (black) ($5{\cdot}10^{-4}$ M in CH_3CN) [(n-Bu)$_4$ N]PF_6] scanned at 0.1 V s^{-1} in the presence of 3 equiv of $H_2PO_4^-$ (red) and in the presence of 3 equiv of $H_2PO_4^-$ and 0.5 equiv of Hg^{2+} (green).

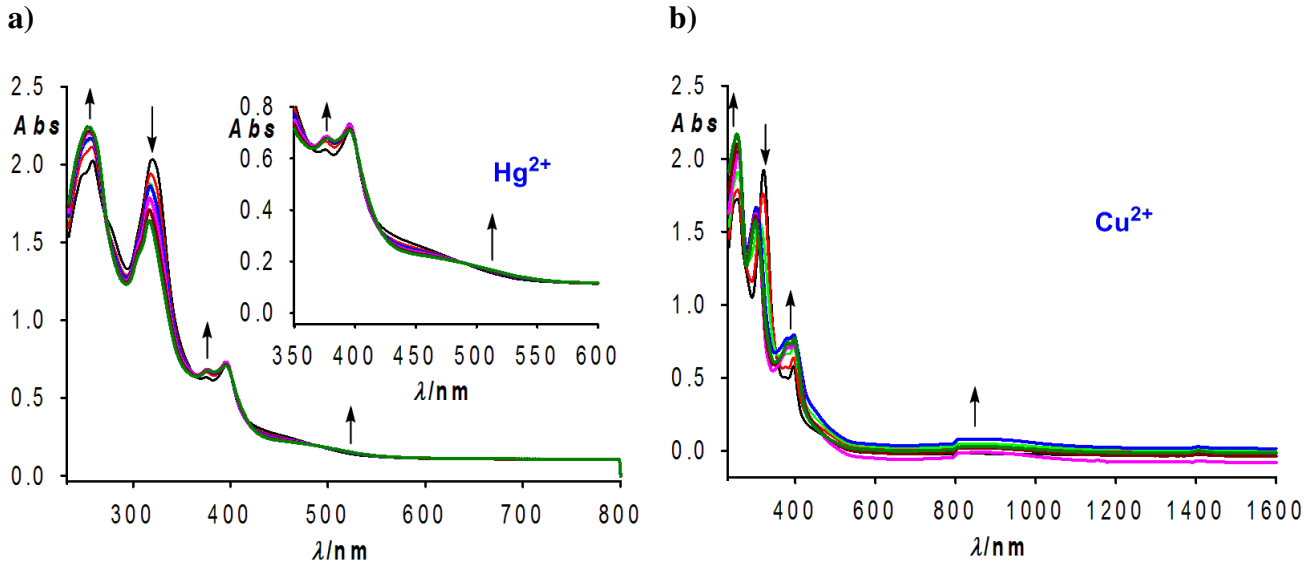

Figure S13. Changes in the absorption spectra of **4** (c = $5{\cdot}x0^{-5}$ M in CH_3CN) upon addition of increasing amounts of (a) $Hg(OTf)_2$; (b) $Cu(OTf)_2$, until 1 equiv was added. Arrows indicate absorptions that increase or decrease during the experiment.

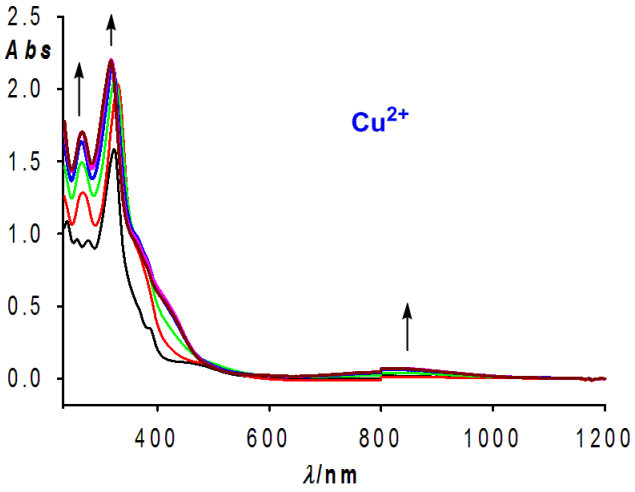

Figure S14. Changes in the absorption spectra of **7** (c = $5 \cdot 10^{-5}$ M in CH_3CN) upon addition of increasing amounts of $Cu(OTf)_2$, until 2 equiv were added. Arrows indicate absorptions that increase or decrease during the experiment.

a) **b)**

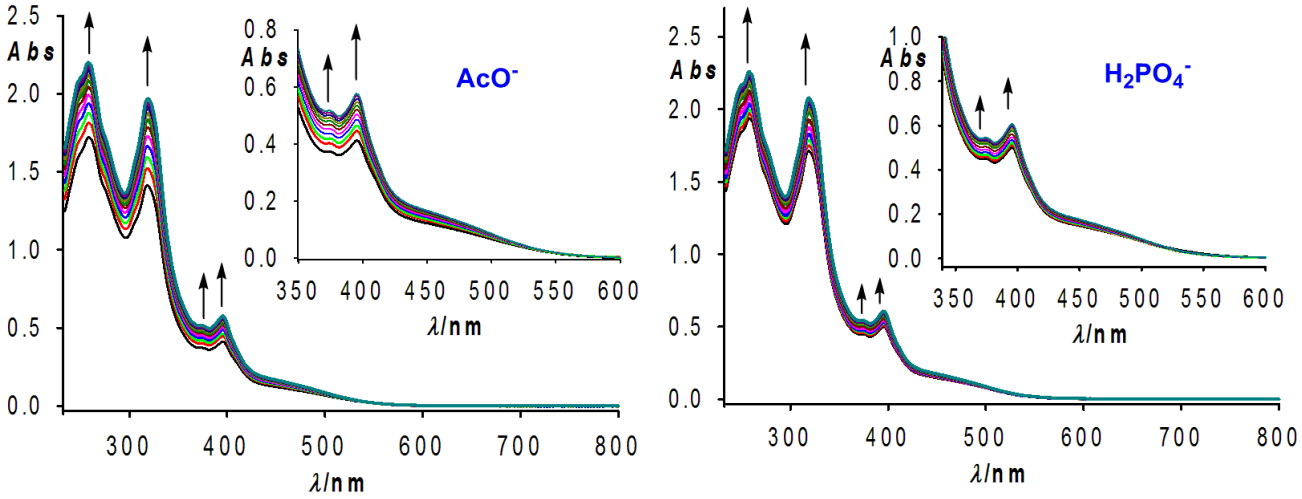

Figure S15. Changes in the absorption spectra of **4** (c = $5 \cdot 10^{-5}$ M in CH_3CN) upon addition of increasing amounts of: (a) AcO^- until 4 equiv were added, (b) $H_2PO_4^-$, until 4 equiv were added. Arrows indicate absorptions that increase or decrease during the experiment.

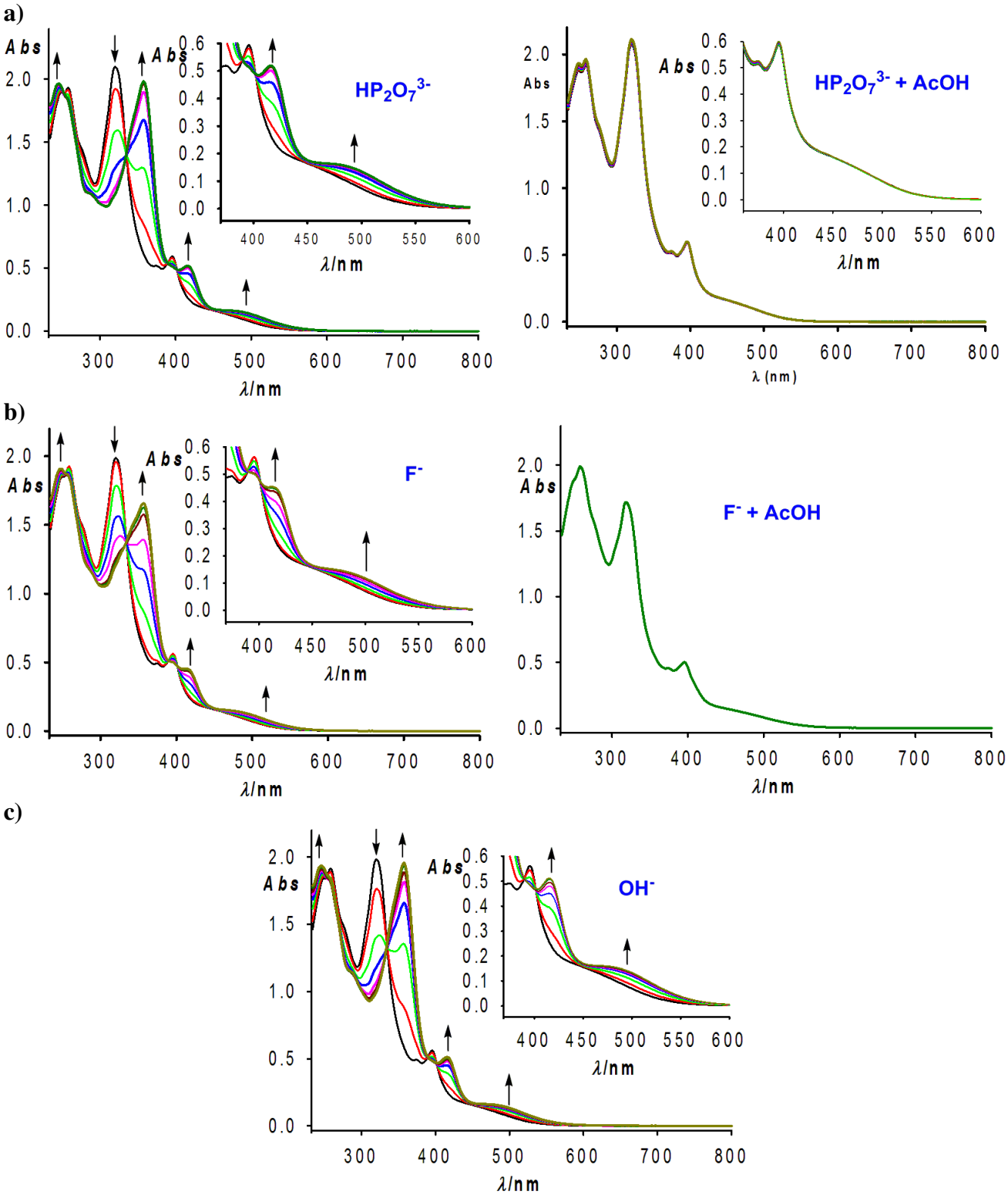

Figure S16. Changes in the absorption spectra of **4** (c = $5x10^{-5}$M in CH_3CN) upon addition of increasing amounts of (a) $HP_2O_7^{-3}$ anion, until 3 equiv (left) and in the present of 20 equiv of acetic acid (right); (b) F^- anion, until 3 equiv (left) and in the present of 20 equiv of acetic acid (right). (c) Changes in the absorption spectra of **4** (c = $5x10^{-5}$M in CH_3CN) upon addition of increasing amounts of OH^- anion. Arrows indicate absorptions that increase or decrease during the experiment.

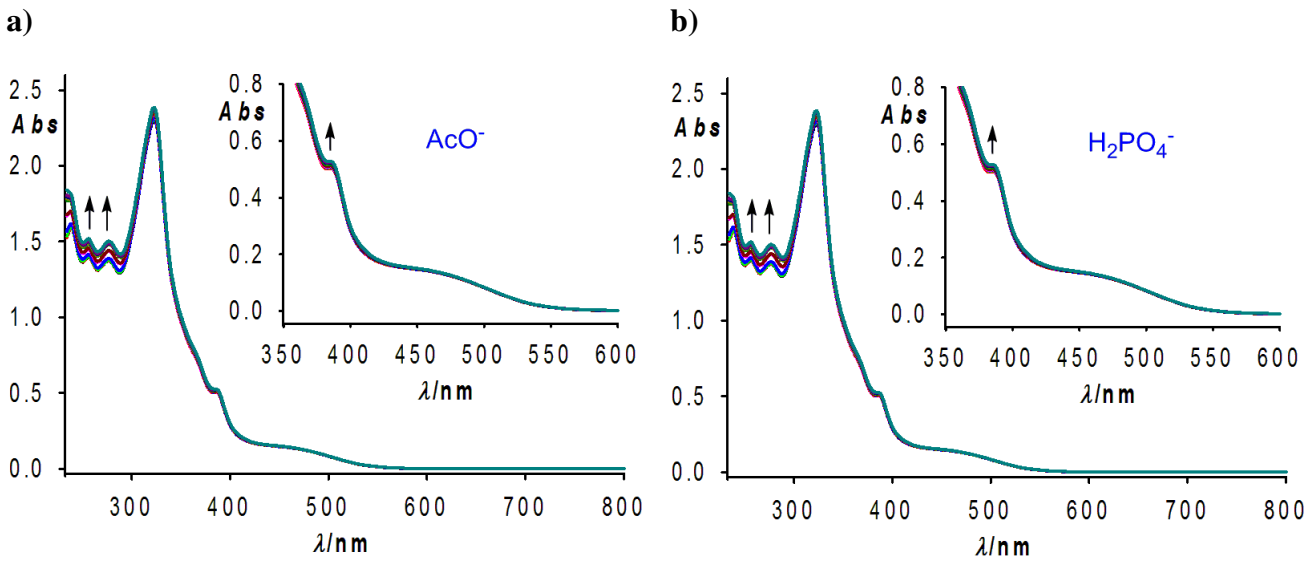

Figure S17. Changes in the absorption spectra of **7** (c = $5 \cdot 10^{-5}$ M in CH_3CN) upon addition of increasing amounts of (a) AcO^-, until 2 equiv were added; (b) $H_2PO_4^-$, until 2 equiv were added. Arrows indicate absorptions that increase or decrease during the experiment.

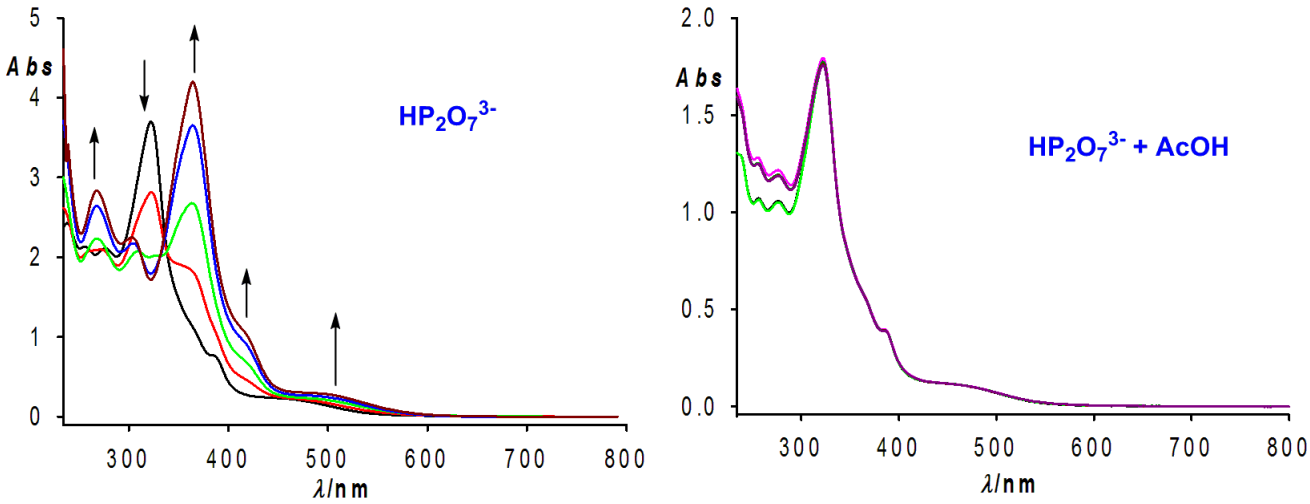

Figure S18. Changes in the absorption spectra of **7** (c = 5×10^{-5}M in CH_3CN) upon addition of increasing amounts of $HP_2O_7^{-3}$ anion, until 3 equiv (left) and in the present of 20 equiv of acetic acid (right). Arrows indicate absorptions that increase or decrease during the experiment.

a)

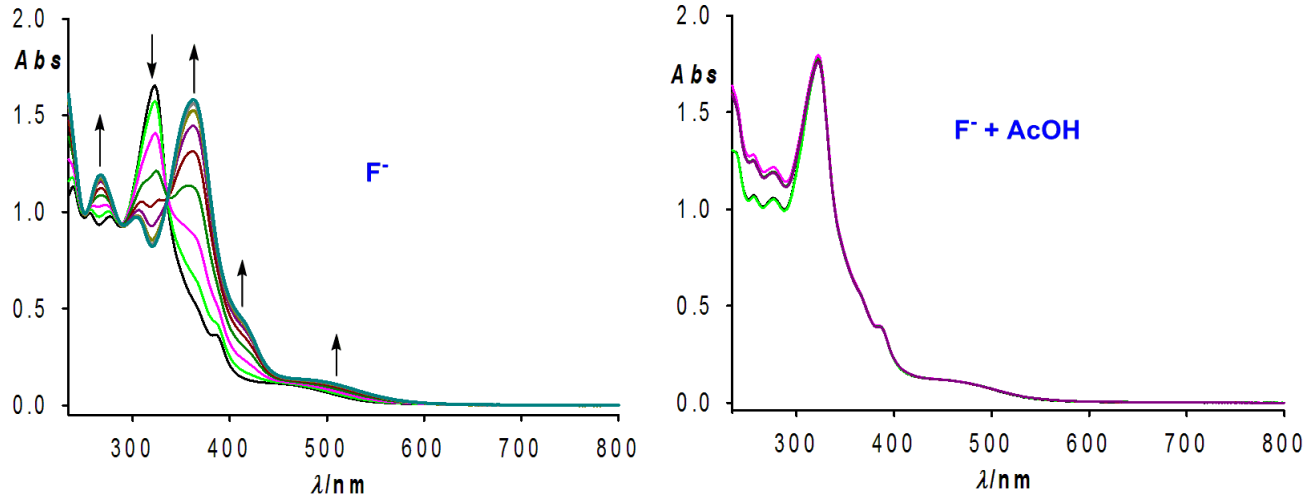

b)

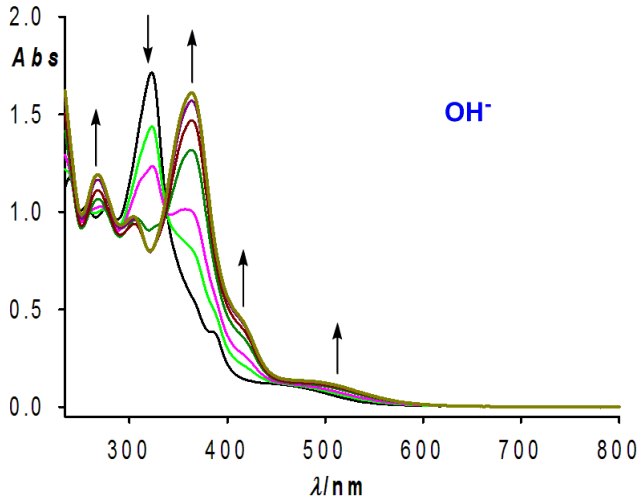

Figure S19. Changes in the absorption spectra of **7** (c = $5x10^{-5}$M in CH_3CN) upon addition of increasing amounts of (a) F^- anion, until 3 equiv (left) and in the present of 20 equiv of acetic acid (right). (b) Changes in the absorption spectra of **7** (c = $5x10^{-5}$M in CH_3CN) upon addition of increasing amounts of OH^- anion. Arrows indicate absorptions that increase or decrease during the experiment.

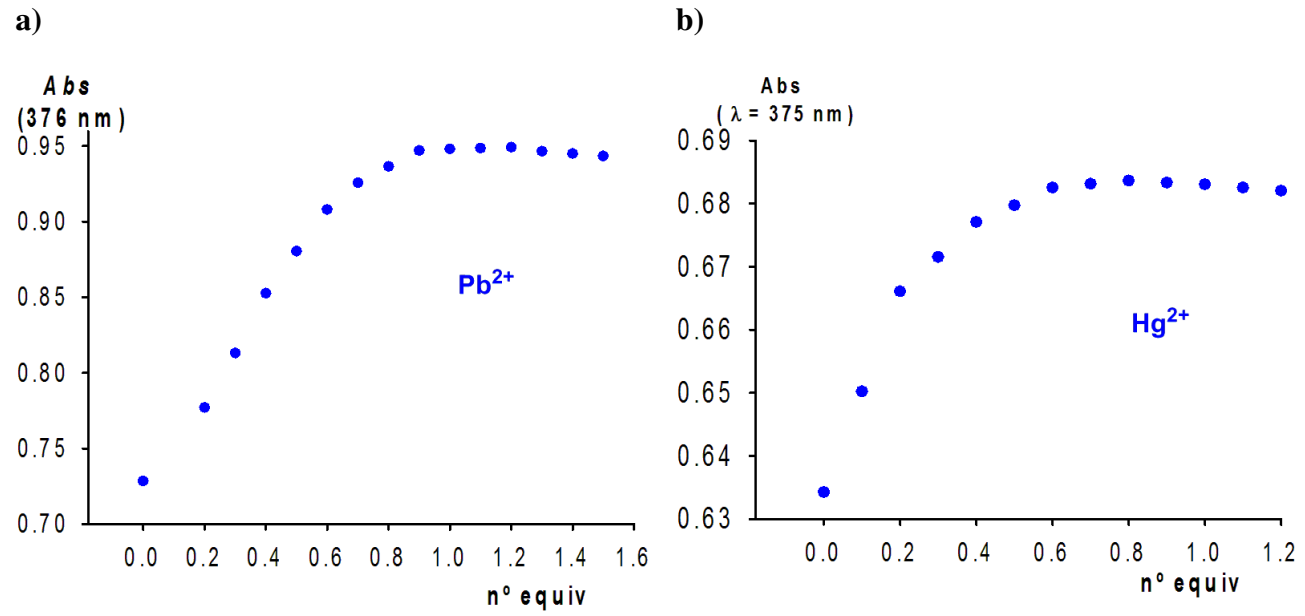

Figure S20. Change of absorbance of **4** (c = $1x10^{-4}$M in CH_3CN) at λ = 375 nm upon addition of (a) Pb^{2+}, indicating the formation of a 1:1 complex; and (b) Hg^{2+}, indicating the formation of a 2:1 complex.

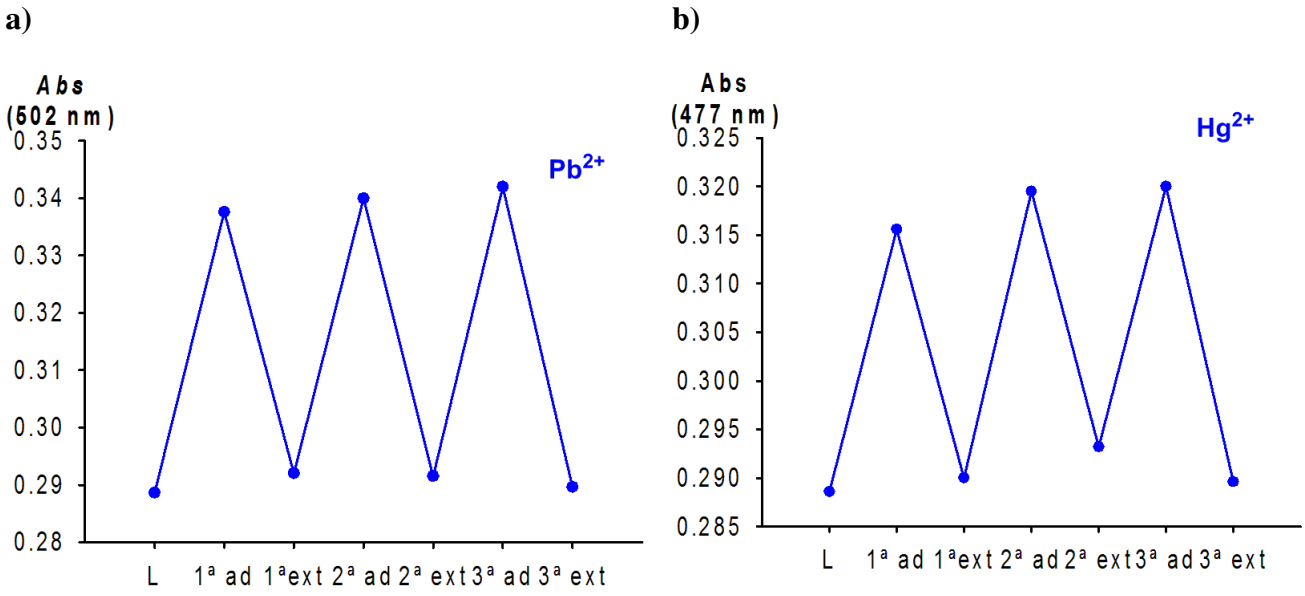

Figure S21. Stepwise complexation/decomplexation (extraction with H_2O) cycles of ligand **4** (c = $1{\cdot}10^{-4}$M in CH_2Cl_2) in the presence of (a) $Pb(ClO_4)_2$ and (b) $Hg(OTf)_2$; carried out by UV/Vis analysis.

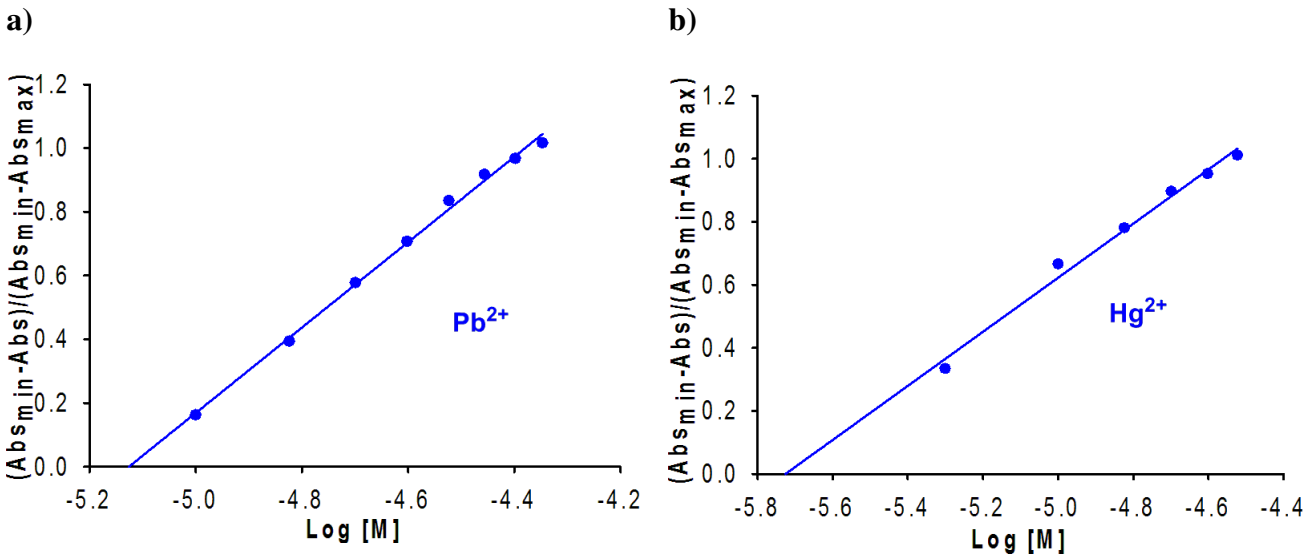

Figure S22. Absorbance of **4** (c = $5x10^{-5}$ M in CH_3CN) at each concentration of cation added (a) $Pb(ClO_4)_2$; (b) $Hg(OTf)_2$, normalized between the minimum absorbance, found at zero equiv of metal cation; and the maximum absorbance, found at (a) $[Pb^{2+}]= 7.47\cdot10^{-6}$ M; (b) $[Hg^{2+}]= 1.22\cdot10^{-6}$ M.

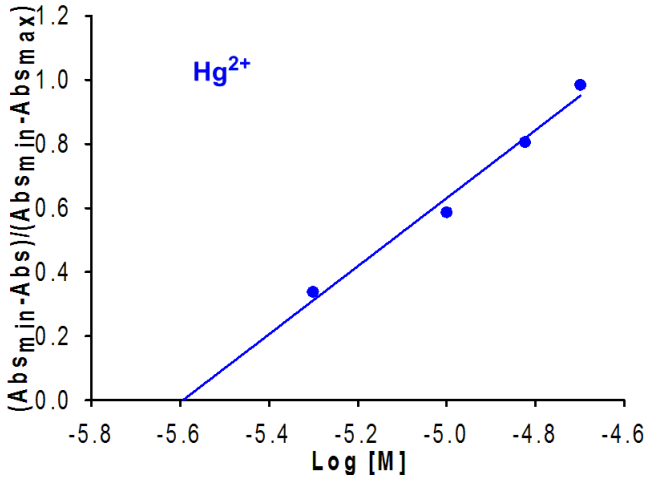

Figure S23. Absorbance of **7** (c = $5x10^{-5}$ M in CH_3CN) at each concentration of cation added $Hg(OTf)_2$, normalized between the minimum absorbance, found at zero equiv of metal cation; and the maximum absorbance, found at $[Hg^{2+}]= 1.55\cdot10^{-6}$ M.

Table S2. UV-vis data of receptor **4** and **7** in the presence of anions.

Comp	UV-vis λ_{max} ($10^{-3}\varepsilon$)[a]	IP[b]
4	320 (1.707); 375 (0.453); 396 (0.496)	
[**4**·AcO^-]	320 (2.216); 375 (0.592); 396 (0.649)	--
[**4**·$H_2PO_4^-$]	320 (2.083); 375 (0.556); 396 (0.612)	--
[**4**·$HP_2O_7^{3-}$]	357 (1.988); 415 (0.523); 485 (0.161)	354, 334, 390, 402
[**4**·F^-]	357 (1.6630); 415 (0.4597); 485 (0.1551)	354, 334, 390, 402
[**4**·OH^-]	357 (1.970); 415 (0.528); 485 (0.165)	354, 334, 390, 402
7	323 (2.448), 385 (0.535)	
[**7**·AcO^-]	323 (2.448), 385 (0.546)	--
[**7**·$H_2PO_4^-$]	323 (2.448), 385 (0.546)	--
[**7**·$HP_2O_7^{3-}$]	304 (0.956), 364 (1.638), 414, (0.458), 500 (0.129)	254, 284, 338
[**7**·F^-]	304 (0.978), 364 (1.585), 414, (0.452), 500 (0.126)	254, 284, 338
[**7**·OH^-]	304 (0.975), 364 (1.609), 414, (0.462), 500 (0.121)	254, 284, 338

[a] λ_{max} in nm, ε in $dm^3mol^{-1}cm^{-1}$; [b] isosbestic points in nm

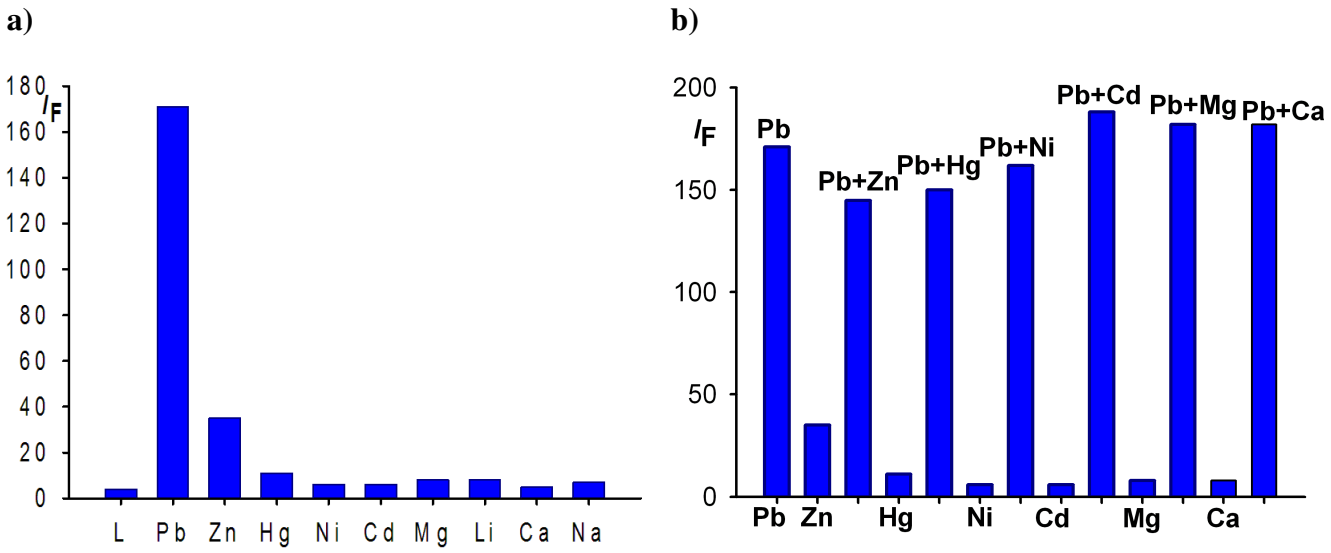

Figure S24. (a) Fluorescente intensity of ligand **4** in CH_3CN, after addition of 1 equiv. of several metal cations. Emission monitored at λ_{exc} = 317 nm. (b) Fluorescence emission intensity of **4** upon addition of 1 equiv. of $Pb(ClO_4)_2$ in the presence of 1 equiv. of interference metal ions in CH_3CN.

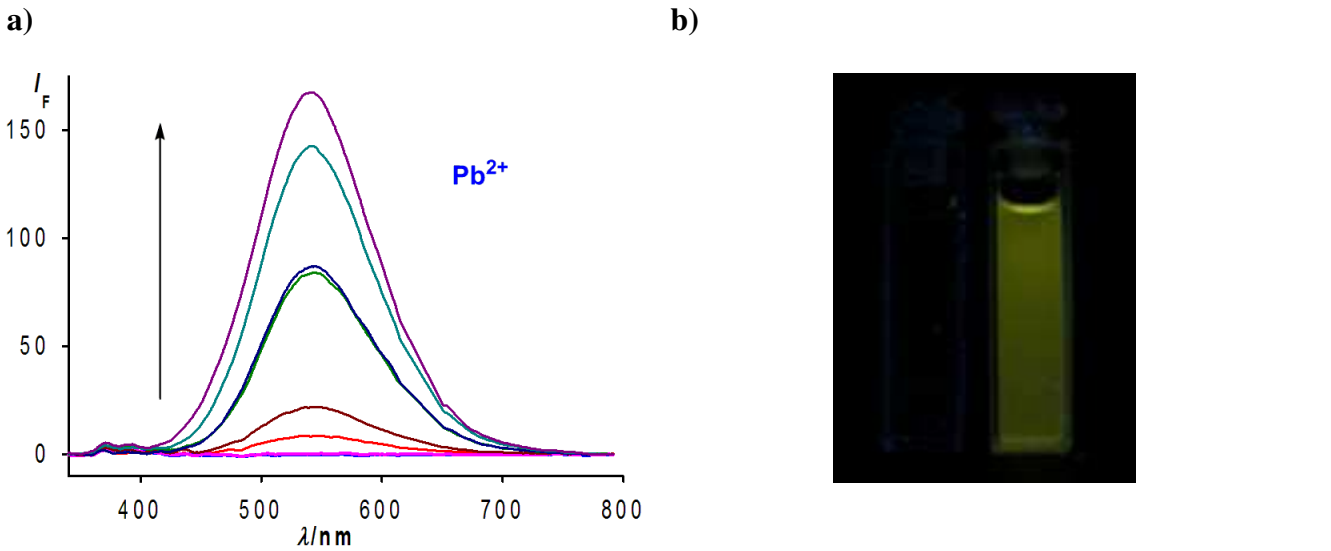

Figure S25. (a) Changes in the fluorescence emission spectrum of **4** (c = $1x10^{-5}$ M in CH_3CN) upon titration with $Pb(ClO_4)_2$: the initial (black) is that of **4** and the final one (deep purple), after addition of 1 equiv. of $Pb(ClO_4)_2$ (c = $2.5x10^{-3}$ M in CH_3CN). Emission is monitored at λ_{exc} = 317 nm. (b) Visual changes observed in the fluorescence of CH_3CN solutions of **4** (left) and after addition of $Pb(ClO_4)_2$ (right).

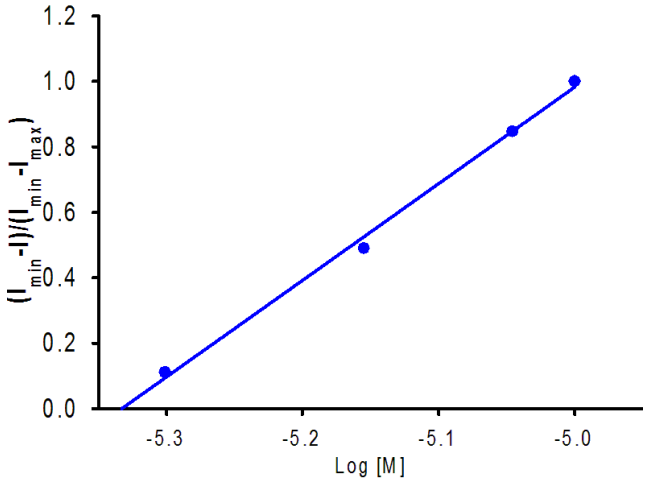

Figure S26. Fluorescence intensity of **4** ($1x10^{-5}$ M in CH_3CN), at each concentration of $Pb(ClO_4)_2$; added, normalized between the minimum fluorescence intensity, found at zero equiv of cation, and the maximum fluorescence intensity, found at $[Pb^{2+}]= 4.64 \cdot 10^{-6}$ M.

Table SI 3. Fluorescence data of receptor **4** in the presence of $Pb(ClO_4)_2$ in CH_3CN solution.

Receptor	λ_{em} (nm)	Φ (CHEF)	Kas (M^{-1})	L.D. (M)
4	520	$3.9 \cdot 10^{-4}$		
[4· Pb^{2+}]	540	0.019 (50)	$3.57 \cdot 10^{6}$	$4.64 \cdot 10^{-6}$

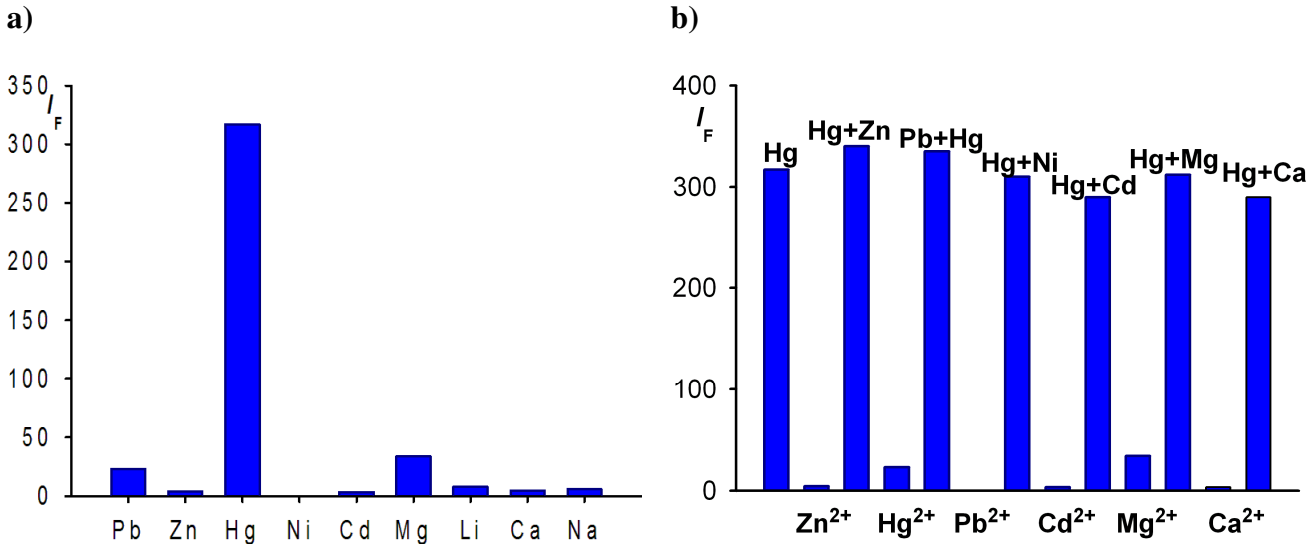

Figure S27. (a) Fluorescente intensity of ligand **7** in CH_3CN, after addition of 2 equiv. of several metal cations. Emission monitored at λ_{exc} = 340 nm. (b) Fluorescence emission intensity of **7** upon addition of 2 equiv. of $Hg(OTf)_2$ in the presence of 2 equiv. of interference metal ions in CH_3CN.

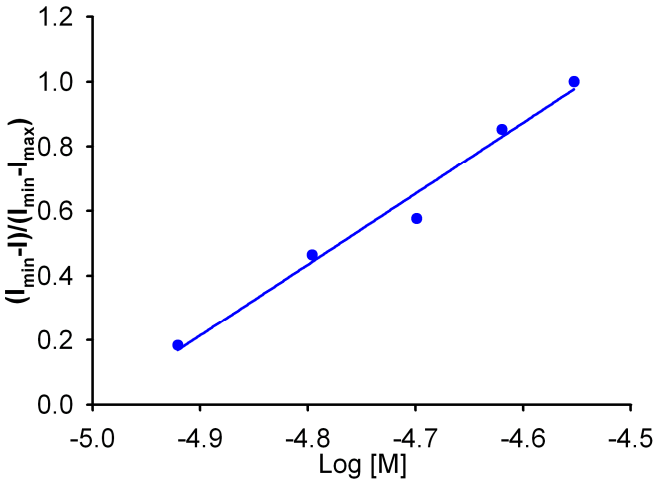

Figure S28. Fluorescence intensity of **7** ($1x10^{-5}$ M in CH_3CN), at each concentration of $Hg(OTf)_2$; added, normalized between the minimum fluorescence intensity, found at zero equiv of cation, and the maximum fluorescence intensity, found at $[Hg^{2+}]= 1.01 \cdot 10^{-5}$ M.

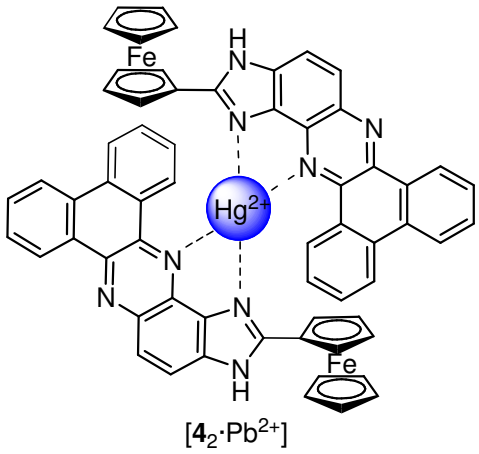

Chart 1. Schematic representation of the binding sites where Hg^{2+} is bound to the receptors **4**.

Table S4. ^{1}H-NMR titration data for receptor **4** in the presence of anions.and cations.

	H^{14}	H^{7}	H^{10}, H^{11}	H^{5}	H^{4}	H^{8}, H^{9}, H^{12}, H^{13}	H^{α}	$H^{\alpha'}$	H^{β}	H^{Cp}
4	9.66	9.41	8.75	8.17	8.10	7.86	5.24	5.17	4.57	4.21

	H^{14} (Δδ)	H^{7} (Δδ)	H^{10}, H^{11} (Δδ)	H^{5} (Δδ)	H^{4} (Δδ)	H^{8}, H^{9}, H^{12}, H^{13} (Δδ)	H^{α} (Δδ)	H^{β} (Δδ)	H^{Cp} (Δδ)
4+Pb^{2+}	9.41 (-0.25)	9.28 (-0.13)	8.67 (-0.08)	8.27 (0.10)	8.06 (-0.04)	7.87 (0.01)	5.35	4.92 (0.35)	4.36 (0.15)
4+$H_2PO_4^-$	9.58 (-0.08)	9.38 (-0.03)	8.72 (-0.03)	8.29 (0.12)	8.04 (-0.06)	7.82 (-0.04)	5.35	4.53 (-0.04)	4.2 (-0.01)
4+AcO^-	9.61 (-0.05)	9.41 (0)	8.74 (-0.01)	8.20 (0.03)	8.01 (-0.09)	7.88 (0.02)	5.29	4.53 (-0.04)	4.18 (-0.03)

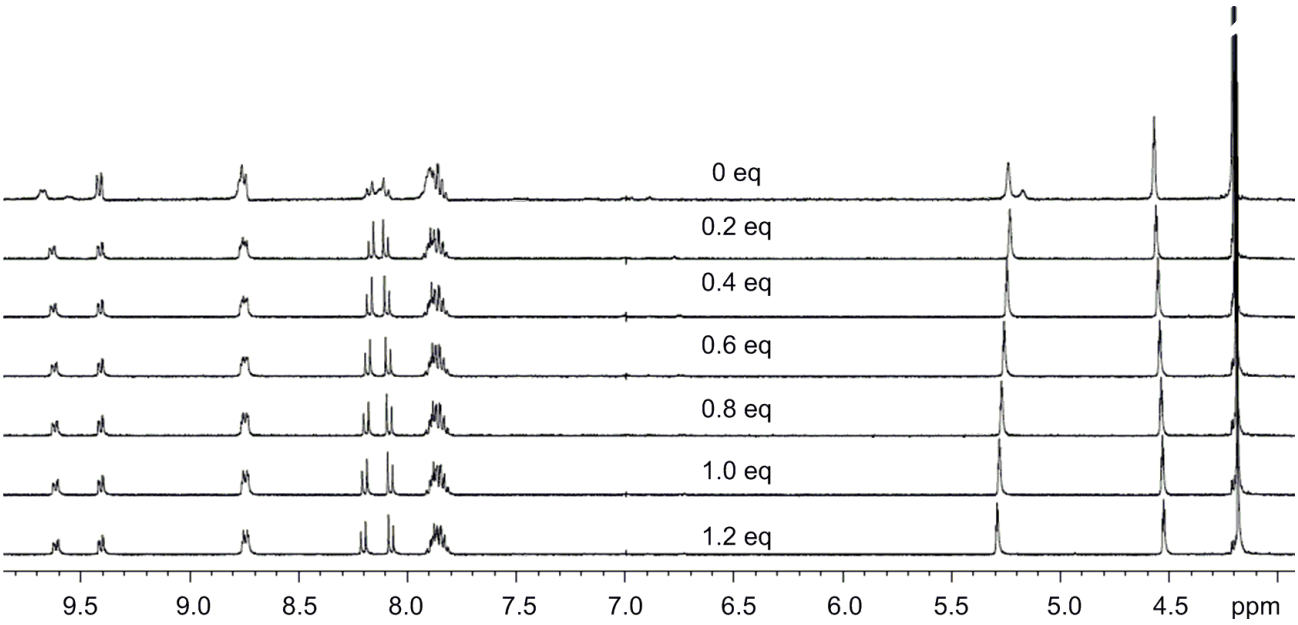

Figure S29. Changes in the ^{1}H-NMR (in acetonitrile-d_3) spectrum of **4** (top) upon addition of increasing amounts of AcO^- until 1.2 equiv (bottom).

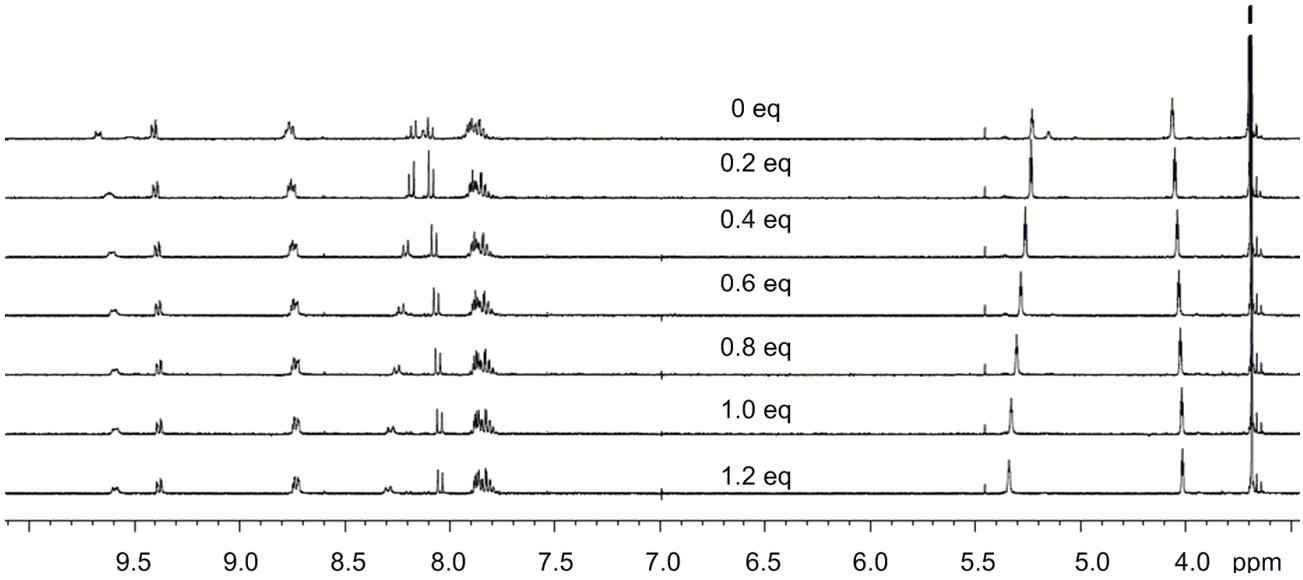

Figure S30. Changes in the ^{1}H-NMR (in acetonitrile-d_3) spectrum of **4** (top) upon addition of increasing amounts of $H_2PO_4^-$ until 1.2 equiv (bottom).

Table S5. ^{1}H-NMR titration data of receptor **7** in the presence of anions.and cations.

	H^9 (Δδ)	H^{12} (Δδ)	H^7 (Δδ)	H^{14} (Δδ)	H^4 (Δδ)	H^5 (Δδ)	H^8 (Δδ)	H^{13} (Δδ)
7	9.79	9.58	9.24	9.20	8.24	8.10	8.01	7.94
7 + Hg^{2+}	10.72 (0.93)	10.05 (0.47)	9.35 (0.11)	9.32 (0.12)	8.56 (0.32)	8.02 (0.38)	8.38 (0.37)	8.24 (0.30)
7 + AcO^-	9.72 (-0.07)	9.57 (-0.01)	9.20 (-0.04)	9.18 (-0.02)	8.27 (-0.03)	8.02 (-0.08)	7.93 (-0.08)	7.93 (-0.01)
7 + $H_2PO_4^-$	9.80 (0.01)	9.59 (0.01)	9.20 (-0.04)	9.17 (-0.03)	8.42 (0.18)	7.98 (-0.12)	7.98 (-0.03)	7.92 (-0.02)

	H^{α} (Δδ)	H_{β} (Δδ)	H^{Cp} (Δδ)
7	5.29	4.57	4.18
7 + Hg^{2+}	5.29 (0)	4.49 (-0.08)	4.13 (-0.05)
7 + AcO^-	5.29 (0)	4.49 (-0.08)	4.13 (-0.05)
7 + $H_2PO_4^-$	5.37 (0.08)	4.45 (-0.12)	4.13 (-0.05)

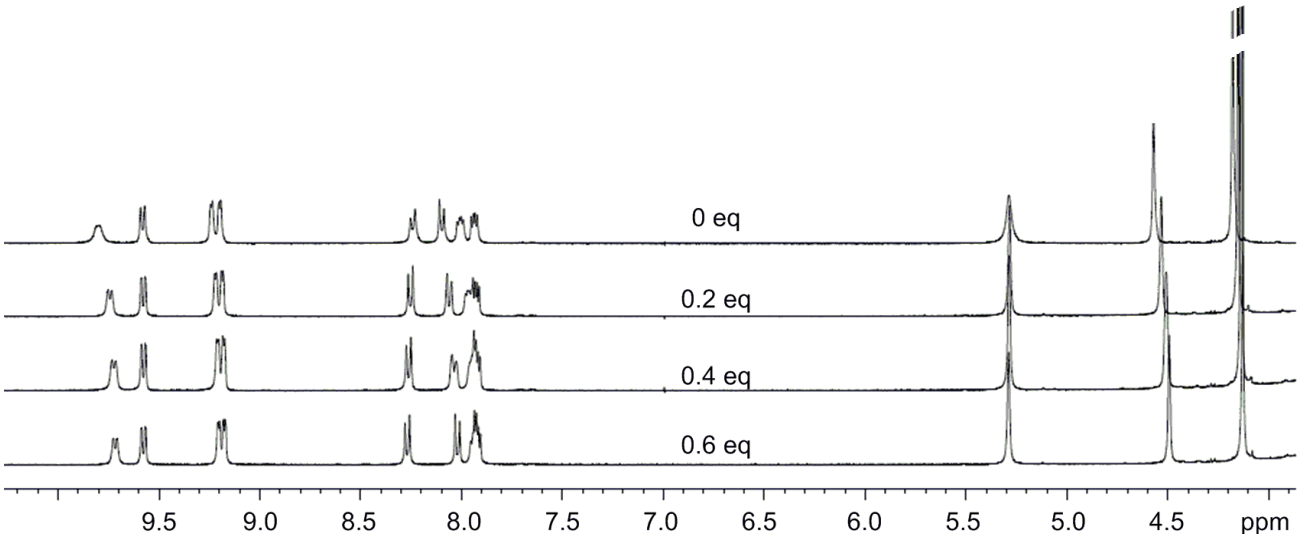

Figure S31. Changes in the ^{1}H-NMR (in DMSO-d_6) spectrum of **7** (top) upon addition of increasing amounts of AcO^- until 0.6 equiv (bottom).

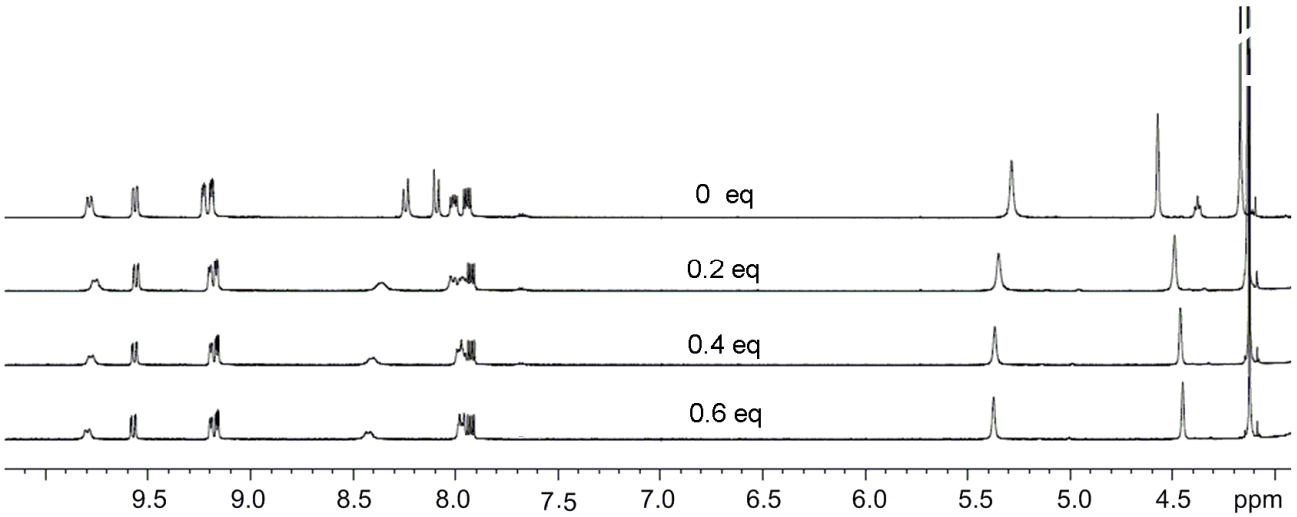

Figure S32. Changes in the ^{1}H-NMR (in DMSO-d_6) spectrum of **7** (top) upon addition of increasing amounts of $H_2PO_4^-$ until 0.6 equiv (bottom).

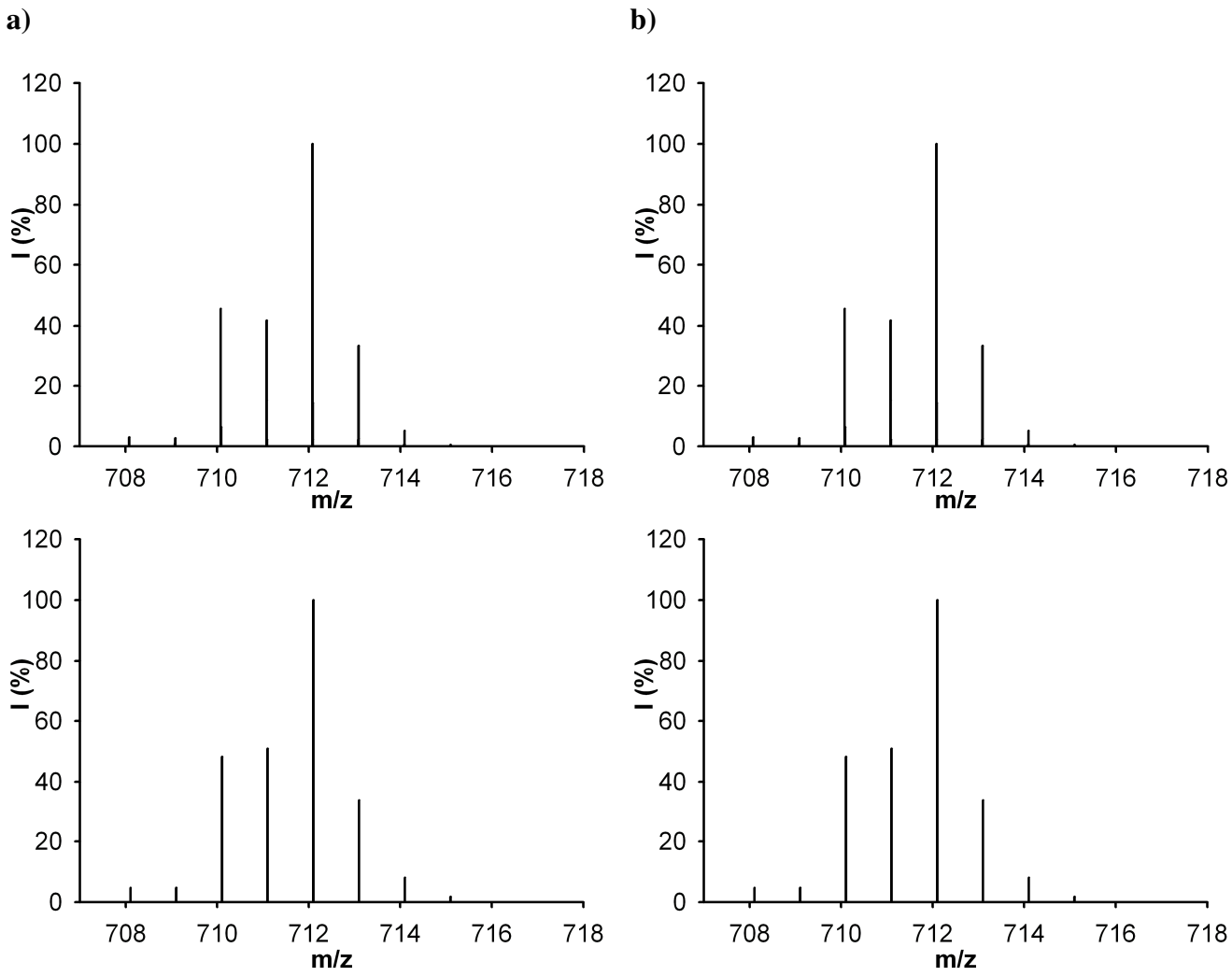

Figure S33. Relative abundance of the isotopic cluster for (a) **4**·Pb^{2+}**;** (b) **4_2·Hg^{2+},** (top) simulated; (bottom) experimental.

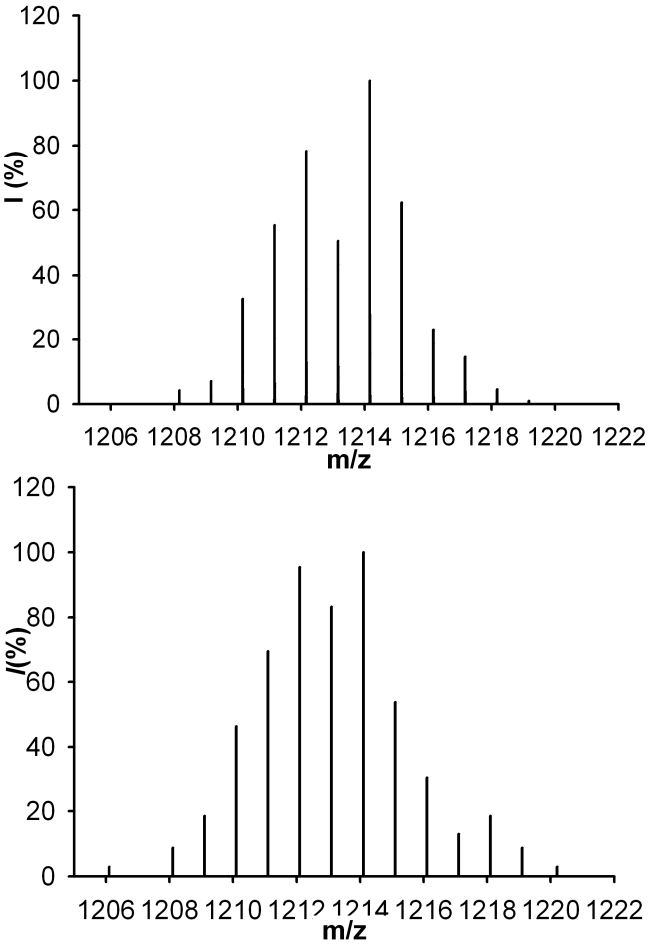

Figure S34. Relative abundance of the isotopic cluster for $\mathbf{4_2 \cdot Hg^{2+}}$, (top) simulated; (bottom) experimental.

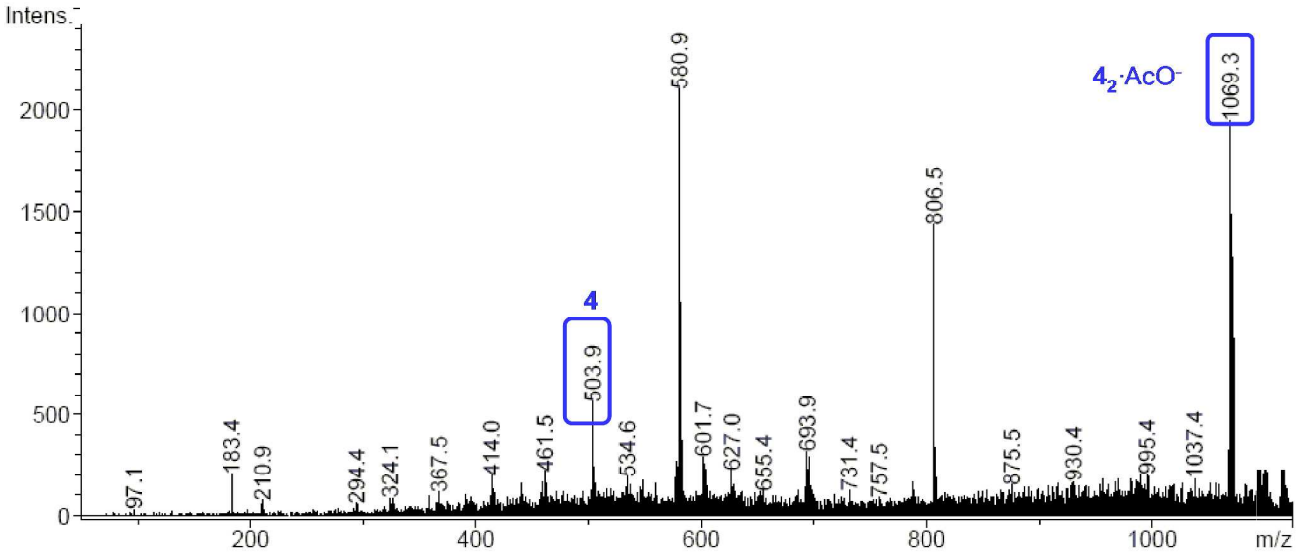

Figure S35. ESI-MS spectra of a acetonitrilo solution of an equimolecular amount of [(n-Bu)$_4$N]AcO and ligand **4**.

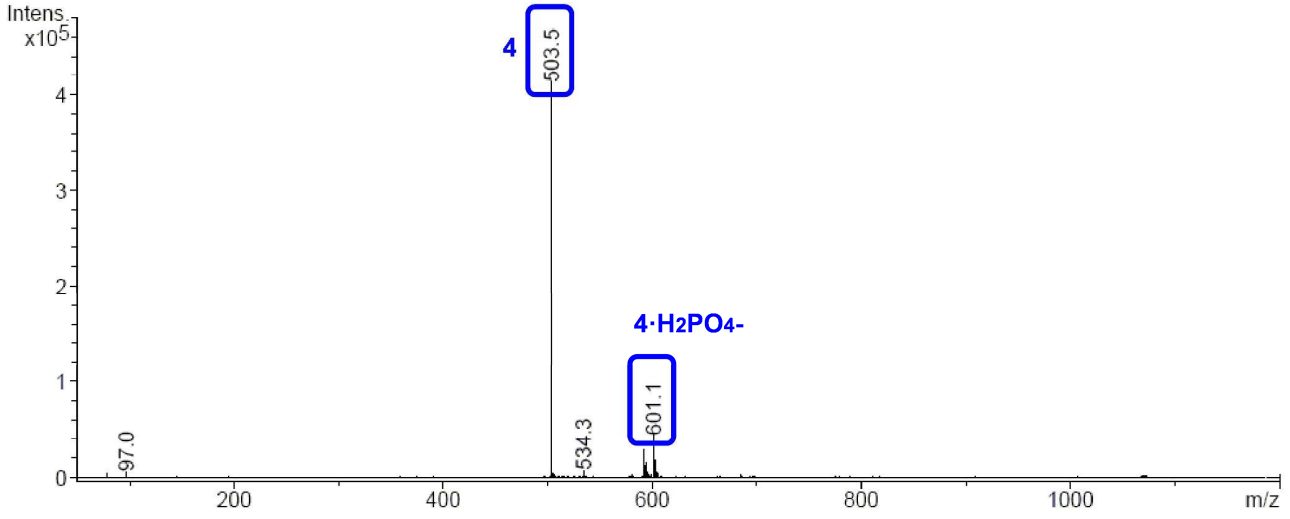

Figure S36. ESI-MS spectra of a acetonitrilo solution of an equimolecular amount of [(n-Bu)$_4$N]H_2PO_4 and ligand **4**.

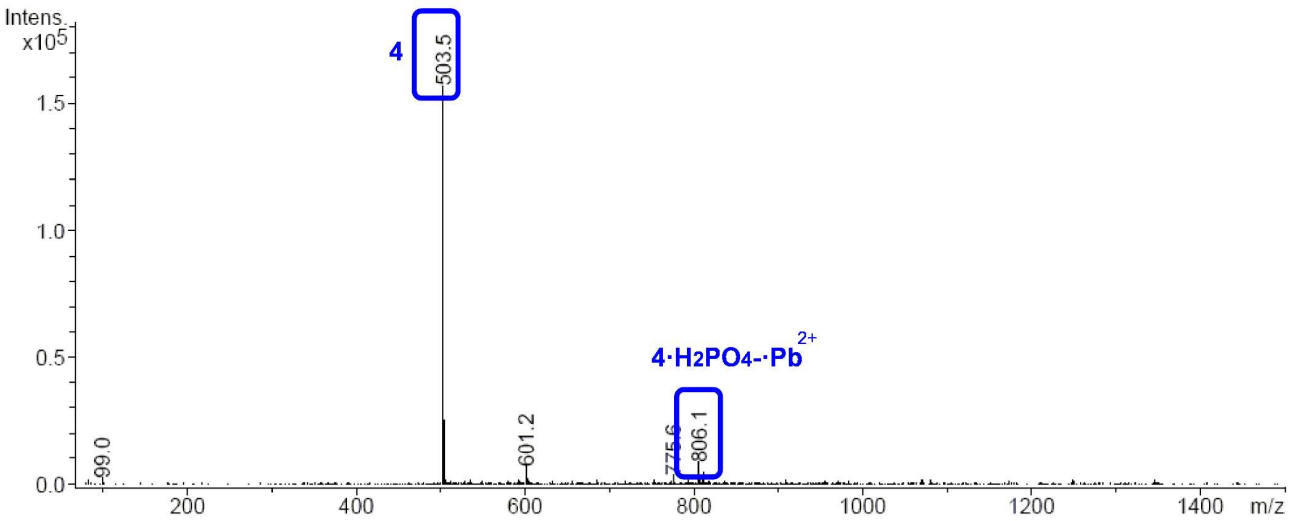

Figure S37. ESI-MS spectra of a acetonitrilo solution of an equimolecular amount of [(n-Bu)$_4$N]AcO, Pb(ClO$_4$)$_2$ and ligand **4**.

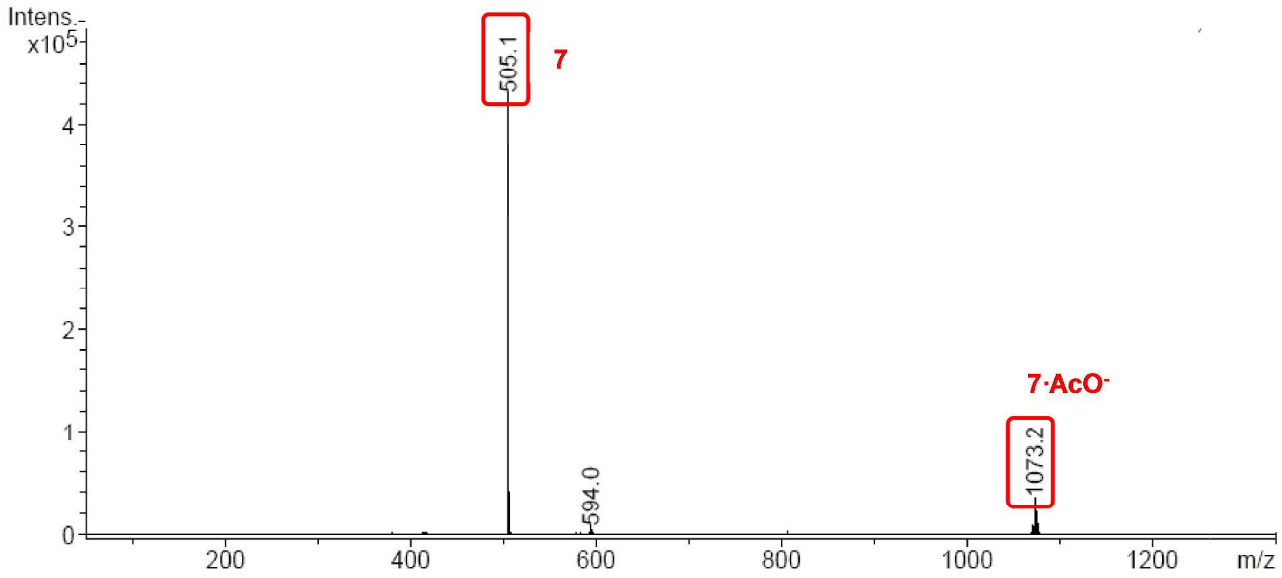

Figure S38. ESI-MS spectra of a acetonitrilo solution of an equimolecular amount of [(n-Bu)$_4$N]AcO and ligand **4**.

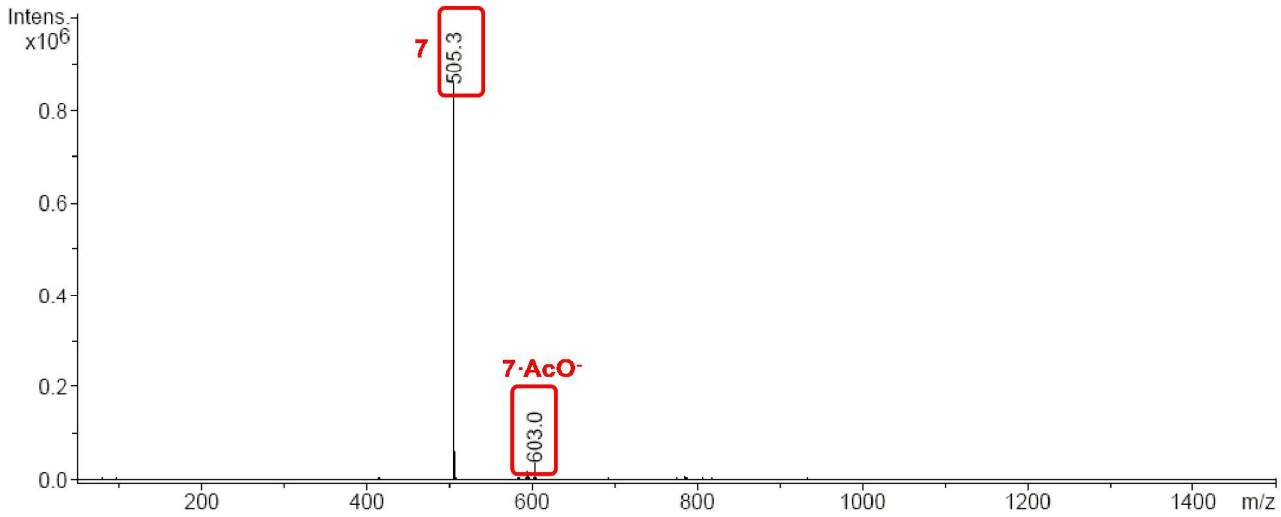

Figure S39. ESI-MS spectra of a acetonitrilo solution of an equimolecular amount of $[(n\text{-}Bu)_4N]H_2PO_4$ and ligand **4**.

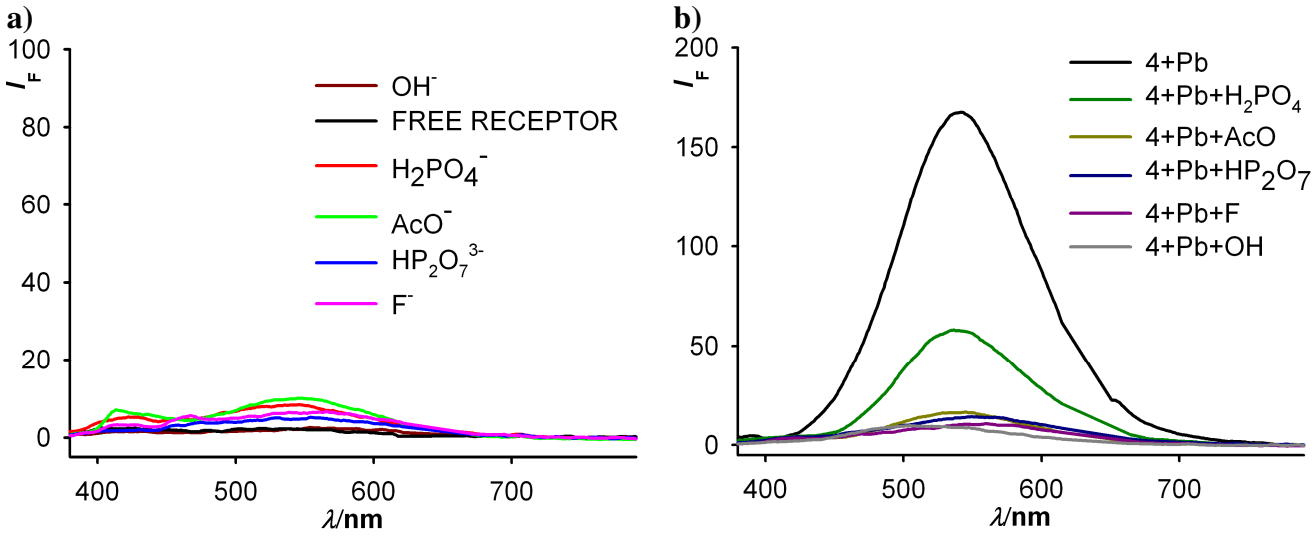

Figure S40. (a) Changes in the fluorescence emission spectrum of **4** (c=1·10^{-5} M in CH_3CN) upon addition of 2 equiv of several anions. Emission monitored at λ_{exc} = 317 nm. (b) Changes in the fluorescence emission spectrum of [**4**·Pb^{2+}] (c=1·10^{-5} M in CH_3CN) upon addition of 2 equiv of several anions. Emission monitored at λ_{exc} = 317 nm

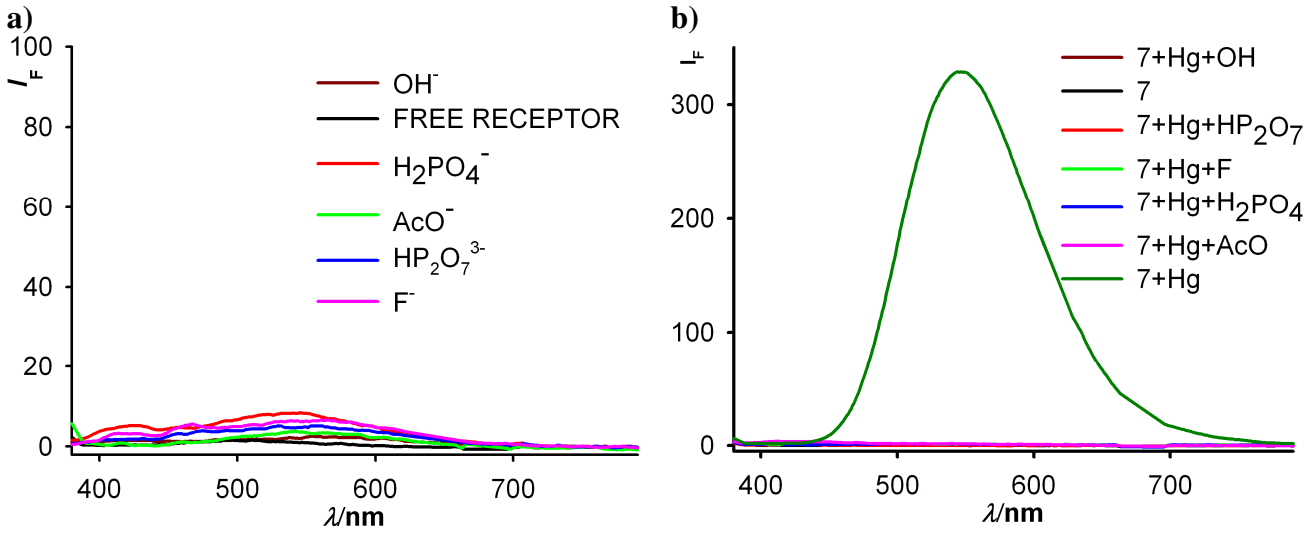

Figure S41. (a) Changes in the fluorescence emission spectrum of **7** (c=1·10^{-5} M in CH_3CN) upon addition of 2 equiv of several anions. Emission monitored at λ_{exc} = 340 nm. (b) Changes in the fluorescence emission spectrum of [**7**·Hg^{2+}] (c=1·10^{-5} M in CH_3CN) upon addition of 2 equiv of several anions. Emission monitored at λ_{exc} = 340 nm.

Experimental Section.-

General Comments.- Melting points were determined on a hot-plate melting point apparatus and are uncorrected. ^{1}H- and ^{13}C-NMR spectra were recorded at 400 and 100 MHz, respectively. Chemical shifts refer to signals of tetramethylsilane in the case of ^{1}H and ^{13}C spectra. The following abbreviations are used to represent the multiplicity of the signals: s (singlet), bs (broad singlet), d (doublet), dd (double doulblets) m (multiplet) st (pseudotriplet), Cq (quaternary carbon atom).

UV-vis spectra were carried out in a UV-vis-NIR spectrophotometer using a dissolution cell of 10 mm path. The samples were solved in CH_3CN ($c = 5x10^{-5}$ M) and the spectra were recorded with the spectra backqround corrected before and after of the sequential additions of aliquots of 0.2 equiv of cations/anions in H_2O ($c = 2.5x\ 10^{-2}$ M).

Fluorescence spectra were carried out in a fluorescence spectrophotometer using a fluorescence cell 10 mm ($c \approx 1x10^{-5}$ M in CH_3CN), as it is stated in the corresponding figure captions. Before recording the spectra, the samples were deoxygenated, to remove fluorescence quenching via oxygen, by bubbling nitrogen for at least 10 min. All the spectra were recorded before and after the sequential additions of aliquots of 0.2 equiv of a solution of cations in H_2O ($c = 2.5x\ 10^{-3}$ M). Quantum yield values were measured with respect to anthracene as standard ($\Phi = 0.27\pm0.01$)[1], using the equation $\Phi_x/\Phi_s = (S_x/S_s)\ [(1-10^{-As})/(1-10^{-Ax})]^2(n_s^2/n_x^2)$ where x and s indicate the unknown and standard solution, respectively, Φ is the quantum yield, S is the area under the emission curve A is the absorbance at the excitation wavelength and n is the index of refraction.

CV and OSWV techniques were performed with a conventional three-electrode configuration consisting of platinum working and auxiliary electrodes and a Ag/AgCl reference electrode. The experiments were carried out with a $\approx 10^{-4}$ M solution of sample in CH_3CN containing 0.1 M (n-$C_4H_9)_4PF_6$ ($TBAPF_6$) as supporting electrolyte. All the potential values reported are relative to the decamethylferrocene (DMFc) couple at room temperature. Deoxygenation of the solutions was achieved by bubbling nitrogen for at least 10 min and the working electrode was cleaned after each run. The cyclic voltammograms were recorded with a scan rate increasing from 0.05 to 1.00 Vs^{-1}, while the OSWV were recorded at a scan rate of 100 mVs^{-1} with a pulse hight of 10 mV and a step time of 50 ms. Typically, receptor (1×10^{-4} M) was dissolved in CH_3CN (5 mL) and $TBAPF_6$ (base electrolyte) (0.190 g) added. The guest under investigation was then added as a $2.5x10^{-2}$M solution in CH_3CN using a microsyringe whilst the cyclic voltammetric properties of the solution were monitored. DMFc was used as an external reference both for potential calibration and for reversibility criteria.

References.-

1.- Dawson, W.R.; Windsor, M.W. *J. Phys.Chem.* **1968**, 72, 3251-3260